

AD-A048 551

CALSPAN CORP BUFFALO N Y  
STUDIES OF HEAT TRANSFER TO GAS TURBINE COMPONENTS.(U)  
OCT 77 M G DUNN, F J STODDARD

F/G 21/5

UNCLASSIFIED

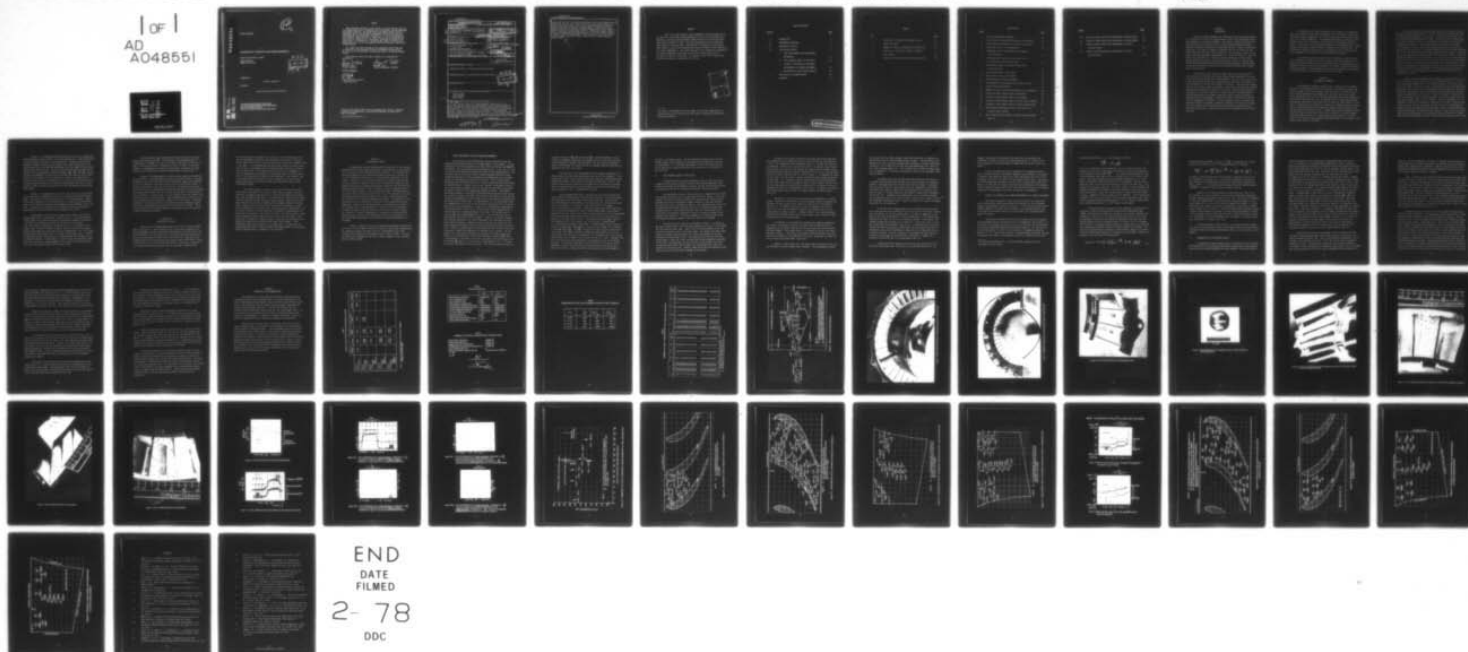
CALSPAN-XE-5933-A-102

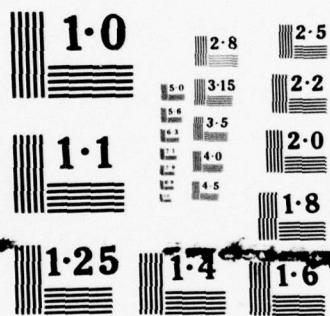
AFAPL-TR-77-66

F33615-76-C-2092

NL

1 OF 1  
AD  
A048551





NATIONAL BUREAU OF STANDARDS  
MICROCOPY RESOLUTION TEST CHART

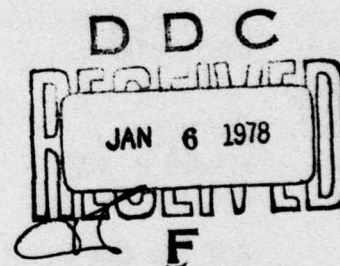
AD A048551

AFAPL-TR-77-66

STUDIES OF HEAT TRANSFER TO GAS TURBINE COMPONENTS

Michael G. Dunn and Frank J. Stoddard

Calspan Corporation  
Buffalo, New York 14221



OCTOBER 1977

June 1976 - October 1977

Final Report

*Approved for public release; distribution unlimited*

AD No.             
DDC FILE COPY

AIR FORCE AERO PROPULSION LABORATORY  
AIR FORCE WRIGHT AERONAUTICAL LABORATORIES  
AIR FORCE SYSTEMS COMMAND  
WRIGHT-PATTERSON AIR FORCE BASE, OHIO 45433

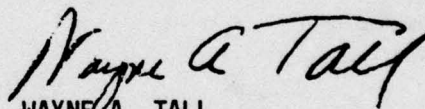
# NOTICE

When Government drawings, specifications, or other data are used for any purpose other than in connection with a definitely related Government procurement operation, the United States Government thereby incurs no responsibility nor any obligation whatsoever; and the fact that the Government may have formulated, furnished, or in any way supplied the said drawings, specifications, or other data, is not to be regarded by implication or otherwise as in any manner licensing the holder or any other person or corporation, or conveying any rights or permission to manufacture, use, or sell any patented invention that may in any way be related thereto.

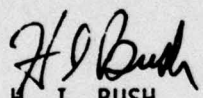
This report has been reviewed by the Information Office (OI) and is releasable to the National Technical Information Service (NTIS). At NTIS, it will be available to the general public, including foreign nations.

This technical report has been reviewed and is approved for publication.

  
KERVYN D. MACH  
Project Engineer

  
WAYNE A. TALL  
Tech Area Manager, Turbines

FOR THE COMMANDER

  
H. I. BUSH  
Deputy Director, Turbine  
Engine Division

Copies of this report should not be returned unless return is required by security considerations, contractual obligations, or notice on a specific document.

Unclassified

SECURITY CLASSIFICATION OF THIS PAGE (When Data Entered)

REPORT DOCUMENTATION PAGE		READ INSTRUCTIONS BEFORE COMPLETING FORM
1. REPORT NUMBER <b>18</b> AFAPL-TR-77-66 ✓	2. GOVT ACCESSION NO.	3. RECIPIENT'S CATALOG NUMBER
4. TITLE (and Subtitle) <b>6</b> STUDIES OF HEAT TRANSFER TO GAS TURBINE COMPONENTS		5. TYPE OF REPORT & PERIOD COVERED <b>9</b> Final Rept. June 76-Oct 77
6. AUTHOR(s) <b>10</b> Michael G./Dunn Frank J./Stoddard		7. PERFORMING ORG. REPORT NUMBER <b>14</b> CALSPAN - XE-5933-A-102 ✓
8. PERFORMING ORGANIZATION NAME AND ADDRESS Calspan Corporation ✓ P. O. Box 235 Buffalo, New York 14221		9. CONTRACT OR GRANT NUMBER(s) <b>15</b> F33615-76-C-2092 ✓
10. CONTROLLING OFFICE NAME AND ADDRESS U.S. Air Force Aero-Propulsion Laboratory (TBC) ✓ Air Force Systems Command Wright-Patterson Air Force Base, Ohio 45433		11. PROGRAM ELEMENT, PROJECT, TASK AREA & WORK UNIT NUMBERS <b>16</b> 30663424 <b>17</b> 04 62203F
12. MONITORING AGENCY NAME & ADDRESS (if different from Controlling Office)		13. REPORT DATE <b>11</b> Oct 77
		14. NUMBER OF PAGES <b>12</b> 46 p.
		15. SECURITY CLASS. (of this report) Unclassified
16. DISTRIBUTION STATEMENT (of this Report) Approved for public release; distribution unlimited		
17. DISTRIBUTION STATEMENT (of the abstract entered in Block 20, if different from Report)		
18. SUPPLEMENTARY NOTES		
19. KEY WORDS (Continue on reverse side if necessary and identify by block number) Turbine blade Heat Transfer Shock-Tunnel		
20. ABSTRACT (Continue on reverse side if necessary and identify by block number) A 180° sector of the first stage stationary inlet nozzle of the AiResearch TFE-731-2 engine was instrumented with thin-film heat-transfer gages and experiments were performed to obtain detailed heat-transfer rate distributions. It is shown that the experimental apparatus can potentially be used to study total-pressure losses in cascades. The experimental apparatus consists of a helium-driven shock tube as a short-duration source of high-temperature high-pressure gas, driving a nozzle test-section device		

DDC  
JAN 6 1978  
F

DD FORM 1 JAN 73 1473 EDITION OF 1 NOV 65 IS OBSOLETE

Unclassified

SECURITY CLASSIFICATION OF THIS PAGE (When Data Entered)

407727

*Incc*

Unclassified

SECURITY CLASSIFICATION OF THIS PAGE(When Data Entered)

mounted near the exit of a primary shock-tunnel nozzle and extending into the shock-tunnel receiver tank. The nozzle test-section device consists of a forward transition section with a circular opening facing the supersonic primary nozzle flow and with the external shape of a frustum of a cone. Internal contouring is provided to transform the circular-section subsonic intake flow into one filling approximately a 180° annular segment having a geometry approximating that of the entrance to the turbine stator stage in a turbojet. Detailed measurements of static pressure in the test section and heat-transfer rate on the stator sector have been obtained and are reported herein.

Unclassified

SECURITY CLASSIFICATION OF THIS PAGE(When Data Entered)

## PREFACE

This is the final technical report prepared by Calspan Corporation on one phase of a multi-phase program sponsored by the Air Force Aero-Propulsion Laboratory, Air Force Systems Command, Wright-Patterson Air Force Base, Ohio, under Contract F33615-76-C-2092. The work reported herein was accomplished under Phase IV of Project 3066, "Investigation of Rotating Stall and Turbine Heat Transfer in Axial Flow Turbomachinery; Phase IV Studies of Heat Transfer to Gas Turbine Components"\*. This particular phase of the program was supported by the Turbine Components Branch and was under the technical direction of Mr. Wayne Tall and Dr. Kervyn Mach. Dr. Michael G. Dunn of the Calspan Corporation was technically responsible for the work.

ACCESSION FOR	
NIS	File Section <input checked="" type="checkbox"/>
DDC	U.I. Section <input type="checkbox"/>
UNANNOUNCED	<input type="checkbox"/>
JUSTIFICATION	
BY	
DISTRIBUTION/AVAILABILITY CODES	
DI	SPECIAL
A	

---

\*The authors are indebted to Mr. Paul Dodge of the Garrett Corporation for supplying the nozzle stators and for many helpful discussions regarding the operating conditions.

## TABLE OF CONTENTS

<u>Section</u>		<u>Page</u>
I	INTRODUCTION	1
II	EXPERIMENTAL APPARATUS	2
III	OPERATION OF FACILITY	5
IV	EXPERIMENTAL RESULTS	7
	A. FLOW ESTABLISHMENT TIME AND PRESSURE MEASUREMENTS	8
	B. TOTAL PRESSURE LOSSES IN TEST DEVICE	10
	C. VALIDITY OF TRANSIENT HEAT-TRANSFER MEASUREMENTS FOR CURRENT EXPERIMENTS	13
	D. PRESENTATION OF HEAT-TRANSFER RESULTS	15
V	CONCLUSIONS AND RECOMMENDATIONS	20
	REFERENCES	47

## TABLES

<u>No.</u>		<u>Page</u>
1	Tabulation of Predicted and Measured Losses	21
2	Stator Vane Data	22
3	Summary of Physical Parameters of Turning Vanes	22
4	Comparison of Axial Heat-Transfer to Surface Heat Transfer	23
5	Summary of Heat-Transfer Data and Gage Locations	24

# ILLUSTRATIONS

<u>Figure</u>		<u>Page</u>
1	Sketch of Experimental Apparatus	25
2	Nozzle Stator Installation in Portion of Test Section	26
3	Turning Vane Installation in Portion of Test Section	27
4	Inlet Stator Prior to Instrumentation	28
5	Photograph of Heat-Transfer Gage Taken Through a Leitz Microscope	29
6	Hole Locations on Airfoil Pressure Side Prior to Installation of Heat-Transfer Gages	30
7	Heat-Transfer Gages in Tip Endwall and Airfoil Pressure Surface	31
8	Heat-Transfer Gages in Tip Endwall	32
9	Heat-Transfer Gages in Hub Endwall	33
10	Reflected-Shock Pressure Measurement	34
11	Total-Temperature Measurements Just Ahead of Stator	34
12	Static-Pressure Measurements	35
13	Summary of Static Pressure Measurements in Test Apparatus	37
14	Location of Heat-Transfer Gages in Hub Endwall	38
15	Location of Heat-Transfer Gages in Tip Endwall	39
16	Location of Heat-Transfer Gages on Airfoil Suction Surface	40
17	Location of Heat-Transfer Gages on Airfoil Pressure Side	41
18	Heat-Transfer Measurement at Gage #3 and Gage #11 on Pressure Side of Airfoil	42
19	Heat-Transfer Rate on Hub Wall, Gage #54 and on End Wall, Gage #30	42

Figure

Page

20	Results of Heat-Transfer Rate Measurement on Stator Endwall	43
21	Results of Heat-Transfer Rate Measurement on Stator Hubwall	44
22	Results of Heat-Transfer Rate Measurement on Airfoil Pressure Surface	45
23	Results of Heat-Transfer Rate Measurement on Airfoil Suction Surface	46

## SECTION I

### INTRODUCTION

In order to achieve maximum cycle efficiencies with gas turbine engines, it is necessary to utilize the maximum possible turbine inlet temperatures within the constraints of structural integrity. The ability to predict accurately the heat-transfer rate distributions for the various engine components therefore becomes an important consideration in achieving this goal. Several calculational techniques, e.g. Dodge [1], Katsanis and McNally [2], Wu [3], Smith [4], and Horlock and Perkins [5] have recently appeared in the literature as have several papers reporting experimental measurements, e.g. Blair [6], Louis [7], Jones and Schultz [8], and Smith [9]. Though the material presented in each of these papers represents an advance in the state-of-the-art, there is a further need for detailed experimental data obtained under known gas-dynamic conditions that can be used to verify the accuracy of the calculation techniques and to supplement the existing data.

At the present time, there are several types of test facilities<sup>6-13</sup> that can be used to perform heat-transfer and/or pressure measurements related to the operation and design of gas turbine engines. The most often used of these is the long run-time steady-state cascade facility and the best approximation to the real problem is the full-scale engine test facility. There are many problems that are well suited to study and solution in these facilities and there are other problems that are difficult or expensive to resolve. With existing steady-flow techniques, it is basically difficult to obtain accurately the detailed heat-transfer distributions on an engine component because a thermal equilibrium is established in these experiments, and the heat-transfer rates must be inferred from the temperature distribution. The test apparatus used for the present experiments provides an important experimental capability fitting between cascade facilities and the full-scale engine facilities because it provides accurate heat-transfer data with a spatial resolution that is comparable with the airfoil thickness.

The purpose of the studies described in this report was to demonstrate that state-of-the-art shock-tube technology and well established transient-test techniques could be successfully used to obtain spatially resolved heat-transfer rates on gas turbine components. For demonstration purposes, these initial experiments used a row of stationary inlet nozzles of the AiResearch TFE-731-2 engine. The facility in which these measurements were obtained provides a clean, uniform, and accurately known gas-dynamic condition at the turbine inlet. The measured heat-transfer distributions can therefore be used to validate and improve confidence in the accuracy of various predictive techniques.

Two technical papers have been written describing the results of this work. Reference 14 contains detailed discussions of the gas dynamics of the transient starting process and flow establishment time associated with the test apparatus utilized in this work and Reference 15 contains a detailed discussion of the heat-transfer rate measurements and resulting distributions on the stator end wall, hub wall, pressure and suction side of the airfoil.

## SECTION II

### EXPERIMENTAL APPARATUS

The experimental apparatus shown in Fig. 1 consists of an 0.203-meter (8-inch) i.d. helium-driven shock tube, which has a 12.19-meter (40-foot) long driver tube and a 15.24-meter (50-foot) long driven tube, as a short-duration source of high-temperature high-pressure gas, driving a nozzle-test-section device mounted near the exit of the primary shock-tunnel nozzle and extending into the shock-tunnel receiver tank. The combination of a large diameter driven tube and very long driver tube accounts for the long test times obtained in this work.<sup>14</sup> The nozzle-test-section device consists of a forward transition section with a circular opening facing the supersonic primary nozzle flow and with the external shape of a frustum of a cone. Internal contouring is provided to transform the circular-section intake flow into one filling a 176° annular segment (maintaining the inviscid cross sectional area nearly constant at a value of  $0.016 \text{ m}^2$  ( $25 \text{ in}^2$ ), and having a geometry approximating that of the entrance to the turbine stator stage in a turbojet.

The forward transition section containing the turbine stator blades is followed by an aft diffuser section. The flow leaving the turbine stator stage has been turned approximately  $69^\circ$  with respect to the axial flow direction before entering the turning-vane stator stage. The function of the turning vanes is to remove a portion of the swirl introduced by the turbine stator blades by turning the flow back  $69^\circ$ . This turning stage was expected to cause large losses because of the very large turning required and because no attempt was made to optimize the design. A discussion presented later in the paper addresses this point. The flow then passes through another transition section in which the flow is transformed from an annular back to a circular cross section. After the turning-vane stator section, the inviscid cross-sectional area is maintained constant at a value of  $0.0122 \text{ m}^2$  ( $18.92 \text{ in}^2$ ) which is less than that of the forward transition section. The diffuser section extends into the shock-tunnel receiver tank and is terminated by a replaceable orifice<sup>16</sup> plate, which provides a means of varying the mass flow and Mach number distribution through the nozzle-test-section device. For the experiments discussed herein the orifice area was  $0.00472 \text{ m}^2$  ( $7.32 \text{ in}^2$ ).

Static pressure measurements were obtained at sixteen locations in the nozzle-test-section device as noted by the circled numbers on Fig. 1. Nine of these measurement locations were in the forward transition section from the inlet to just ahead of the stator blades, three measurements were made immediately downstream of the stator tip exit, three measurements were made just downstream of the flow straighteners, and one measurement was made approximately one duct diameter upstream of the orifice plate. Figure 2 illustrates a portion of the test section and the nozzle stator installation but with the external cone and outer contour parts, shown in Fig. 1, removed. From this photograph, the circumferential locations of the pressure transducers at two axial locations ahead of the stator can be seen. The center stator section in this photograph was replaced with one containing the thin-film gages in order to perform the heat-transfer measurements. Also shown on this figure is a rake of ten total temperature probes (see Bontrager [17]) containing 0.0005-inch diameter butt-welded chromel-alumel thermocouples housed in 0.050-inch diameter stainless steel tubes.

Figure 3 is a photograph taken from downstream of the flow straighteners discussed earlier in this section. As was the case for Fig. 2, the outer portion of the test section (see Fig. 1) has been removed. The position of the three pressure transducers located at 0.0165-meters (0.65-inches) downstream of the turning vanes can be seen from this photograph as can the contour of the turning vanes and the aft bullet nose. The three lead wires shown exiting from the top surface of the large diameter housing and numbered (14), (15), and (16) come from the pressure transducers located on the tip surface near the exit of the stator and prior to the entrance of the turning vane. Figure 3 also demonstrates a fillet that was placed at the junction of the aft bullet nose and the flat plate. A similar fillet was used at all junctions of mating parts with the flat plate surface in order to minimize the potential for flow disturbances resulting from sharp corners.

Figure 4 is a photograph of one of the stator nozzles as received from Garrett and prior to machining the holes for installation of the heat-transfer gages. These stators had been used previously in an operating engine. Because the relative importance of film cooling was not of interest in the present program, all the cooling-air passages were plugged and faired smoothly into the contour. In addition, the three small bosses shown near the flat surface were ground smooth in order to prevent test-gas leakage in the system.

A photograph of one of the heat-transfer gages used in this work was taken through a Leitz microscope and is shown in Fig. 5. These thin-film heat-transfer gages were constructed using well-established techniques described by Vidal [18]. The insulating substrate for the metallic film is pyrex  $9.65 \times 10^{-4}$  meters (0.038-inches) in diameter by  $7.112 \times 10^{-4}$  meters (0.028-inches) thick. The thin-film gage is made of platinum ( $\sim 1000$  Å thick) and is painted on the substrate in the form of a strip approximately  $1.016 \times 10^{-4}$  meters (0.004-inches) wide by about  $5.08 \times 10^{-4}$  meters (0.020-inches) long. A coating of magnesium fluoride ( $\sim 1200$  Å thick) is vapor deposited over the gage to protect against abrasion. A diamond drill was used to notch the substrate on each side, (as can be seen on the photograph) so as to permit the lead wires access to the thin film without contact with the metal nozzle.

The heat-transfer gages described above were installed in the stator nozzle at 58 selected locations. The holes were electro-machined and were counterbored to a diameter of  $1.016 \times 10^{-3}$ -meters (0.040-inch) by  $8.128 \times 10^{-4}$ -meters (0.032-inch) deep with a through hole  $5.08 \times 10^{-4}$ -meters (0.020-inch) diameter. A photograph of the stator illustrating the construction of these holes prior to installation of the heat-transfer gages is shown in Fig. 6.

Figures 7-9 are photographs of the heat-transfer gage installation for the tip end wall, the airfoil pressure surface and the hub end wall. From these photographs, the relative locations of the heat-transfer gages can be observed as can the orientation of the gage elements relative to the stator surface. It should be noted that in some areas of the airfoil, the material was not sufficiently thick to allow counterboring in which case the hole was machined through. Of the heat-transfer gages that were installed in the stator, 23 were placed in the tip end wall, 7 in the hub wall, 16 on the pressure side of the airfoil, and 12 on the suction side of the airfoil. Detailed measurements of the hole locations were made and these locations are given later in this report. During the experiments, a constant current of 1 milliamperes was passed through the gages which have a room temperature resistance on the order of 50 to 100  $\Omega$ . The resulting  $i^2R$  heating of the gage produced an insignificant part of the gage  $\Delta T$  experienced during an experiment.

### SECTION III

#### OPERATION OF FACILITY

Operation of the Turbine-Blade-Heating Test Facility follows standard shock-tunnel practice. The shock-tunnel flow is initiated by rupturing the double diaphragms initially separating the high-pressure helium driver gas from the low-pressure air in the driven tube. The primary shock wave generated in the air test gas reflects from the end of the driven tube, rupturing a mylar diaphragm between the driven tube and the evacuated shock-tunnel nozzle, thereby initiating the air flow in the shock-tunnel nozzle. Several wave reflections occur between the driven-tube end wall and the helium/air interface until

equilibrium-interface conditions<sup>19</sup> are achieved in the reflected-shock reservoir and subsequent steady-flow nozzle conditions are achieved. This gas-dynamic behavior can be seen in the reflected-shock pressure data presented later in this paper. At a predetermined time after shock reflection from the shock tube end wall, a centerbody valve is actuated and seals off the test section from the shock tube. In this manner, the potential for tiny fragments of metal diaphragm particles damaging the heat-transfer gages is reduced significantly. Past experience has shown that this technique is very effective and it was demonstrated to be so here in that no damage to any of the 58 heat-transfer gages used in this work was experienced during the course of the experimental program.

The initial unsteady supersonic nozzle flow enters the nozzle test-section device and chokes at the turbine stator throat, causing a reflected shock wave to propagate upstream until it issues from the mouth of the device. Part of the incoming shocked flow is spilled around the forward conical frustum and part enters the circular opening at subsonic speeds. When the shock wave exits from the test section, an expansion wave propagated towards the stator. After a complex series of internal and external wave interactions, a steady flow is established in the device with a detached bow wave standing ahead. The aft portion of the test section experiences a different starting process because there are essentially two orifices in series. The initial shock is transmitted through the stator throat and reflects from the orifice plate. This reflection is followed by a complex series of reflections and expansions until steady-state conditions are achieved after about 9 milliseconds. A one-dimensional analysis was used prior to the experiments to estimate the flow establishment time and the results indicated that approximately 7 milliseconds would be required which is considered to be consistent.

#### SECTION IV EXPERIMENTAL RESULTS

An experimental program demonstrating the feasibility of the technique described herein for obtaining detailed spatial distributions of heat-transfer rate on full-scale engine components has been completed. The reflected-shock reservoir conditions in the equilibrium interface region were a pressure of  $1.51 \times 10^7$  newtons/m<sup>2</sup> (2190 psia) at a reflected-shock temperature of 1570°K (2825°R). Figure 10 is an oscilloscope record of the pressure data from two of the four pressure transducers used in the reflected-shock region for each experiment from which the equilibrium interface conditions were obtained using standard shock-tube tables<sup>20</sup> and by assuming an isentropic compression after the initial shock reflection. For the measured incident shock Mach number of 3.39 and the initial driven-tube pressure of  $1.86 \times 10^5$  newtons/m<sup>2</sup> (26.9 psia), the measured reflected-shock pressure for the initial 3 milliseconds after shock reflection is in excellent agreement with theory. The theoretical value of entropy was used to perform the calculation of the equilibrium interface temperature. Because of the gradual pressure rise during the test period, it was necessary to use an average pressure to calculate reservoir conditions. No attempt was made to vary the driver gas He/Air ratio in order to improve this situation. Previous<sup>21</sup> measurements at Calspan of the reflected-shock radiation-intensity history have demonstrated that for helium driving air at low incident shock Mach numbers the equilibrium interface approximation is acceptable.

Figure 11 illustrates the total-temperature measurements obtained with two of the  $1.27 \times 10^{-5}$ -meter (0.0005-inch) diameter chromel-alumel thermocouples. The temperature deduced from these traces for thermocouple #9 was 1530°K (2750°R) and that deduced for thermocouple #10 was 1400°K (2520°R). The average measured total temperature was 1440°K (2600°R) compared to the calculated value of 1570°K (2825°R).

#### A. FLOW ESTABLISHMENT TIME AND PRESSURE MEASUREMENTS

The test-section flow establishment time was calculated using one-dimensional gas-dynamic relations to be approximately 7 milliseconds. A brief description of the starting process was given earlier in the section OPERATION OF FACILITY. The static pressure data presented in Figs. 12 (a), (b), (c), and (d) can be used to confirm the qualitative nature of the starting process. The sweep rate for all of the oscilloscope records presented herein was 5 milliseconds/cm which was too slow for quantitative determination of the starting process but acceptable for qualitative discussion. Each of these pressure transducers has a different sensitivity so that the absolute deflections cannot be compared directly. However, later in this section, the pressure results at the various locations through the device are presented and they are discussed in detail in terms of losses experienced through the device. The pressure measurement obtained at station (1) illustrates both the arrival of the initial wave system at slightly more than 2 milliseconds after sweep initiation and the arrival at approximately 2.5 milliseconds later of the shock wave reflected from the turbine stator-stage throat. At approximately 2.5 to 3 milliseconds later, the expansion wave as a result of the shock wave leaving the device can be seen. After several wave interactions, a steady flow is established at approximately 9 milliseconds after arrival of the initial pressure signal suggesting that a detached bow wave is established ahead of the inlet. The pressure data at locations (2), and at (5) and (6) shown in Fig. 12 (b) are also shown to be qualitatively consistent with this argument. Figure 12 (c) presents pressure data obtained downstream of the flow straighteners and illustrates the transmitted shock followed by a compression wave system that is a mixture of waves being transmitted through the stator and those being reflected from the orifice plate. However, at approximately 9 milliseconds after the arrival of the transmitted shock, steady-flow conditions are obtained at this location. The subsequent 8 or 9 milliseconds represent the available test time in the device. Figure 12 (d) illustrates the pressure data obtained at location (13), which is approximately 0.116-meters (4.55-inches) upstream of the orifice plate, and at location (14) which is in the tip wall at approximately  $2.54 \times 10^{-3}$ -meters (0.10-inches) downstream of the stator exit. The initial transmitted shock can

be seen to arrive at (14) earlier than at (13) as would be expected. The influence of subsequent compression and expansion waves are seen in the pressure history during the transient starting process, but once again after approximately 9 milliseconds, the pressure reaches a reasonably uniform value which is designated test time on the figure.

The results of static measurements for five separate experiments are shown on Fig. 13 for the seven measuring stations in the test apparatus. It is illustrated on Fig. 1 that at each of four axial locations, three pressure measurements were taken in the azimuthal direction (see also Figs. 2 and 3). The measured static pressure variation with azimuth was on the order of 1 percent, which is within the accuracy of the transducers, and thus all of the data are plotted together on Fig. 13 independent of location.

Using one-dimensional theory, the known area of the aft diffuser and orifice plate, and the measured static pressures from Fig. 13, one can calculate the Mach number in the aft diffuser and the mass flow rate. The results of this calculation give a Mach number in the aft portion of 0.236 and a mass flow rate of 3.50 Kgm/sec (7.72 lb/sec) for the 176° sector of 7.17 Kgm/sec (15.8 lb/sec) for the full turbine. Knowing the forward area and the mass flow rate, an iteration technique was used to find the Mach number in the forward section ahead of the stator to be 0.15 at a total pressure of  $8.74 \times 10^5$  newtons/m<sup>2</sup> (126.8 psia) giving a flow velocity of 114.15 m/sec (374.5 ft/sec) and a gas density of 1.922 Kgm/m<sup>3</sup> (0.12 lb/ft<sup>3</sup>). The resulting Reynolds number ahead of the stator was  $4.27 \times 10^6$  per meter ( $1.3 \times 10^6$  per foot) or approximately  $1.3 \times 10^5$  based on mid annular chord length. The Mach number at the stator exit tip was calculated to be approximately 0.7 based on the average static pressure at locations (14), (15), and (16), divided by the total pressure ahead of the stator inlet. The stator stage was designed for a Mach number of 0.8 at this location and a mass flow rate of approximately 13.61 Kgm/sec (30 lb/sec) for the entire turbine or 6.65 Kgm/sec (14.67 lb/sec) for the 176° sector. Therefore, the mass flow rate used in these experiments was approximately half of the design condition. In subsequent experiments, the mass flow will be increased to the appropriate value by increasing the shock-tunnel primary nozzle throat area which has the effect of moving the inlet pick-off point to the Mach number 4.0

location in the primary nozzle. For the experiments reported here, the pick-off Mach number was approximately 4.5 and the post-shock specific heat ratio was approximately 1.3. The design Mach number of 0.8 at the stator exit tip can be achieved by increasing the orifice size which also will increase the mass flow rate.

#### B. TOTAL PRESSURE LOSSES IN TEST DEVICE

The measured static pressures presented in Fig. 13 were then used in conjunction with existing literature results (Balje [22]) to demonstrate that the device used here was performing as expected and that the same device may be a potentially useful one for studying total-pressure losses in cascades.

The experimental values of total pressure were computed from the weight flow obtained by assuming that the downstream orifice was choked, by using the average of the static pressures measured just upstream of the orifice, and by assuming that the total temperature remains constant, at the value measured near the stator inlet, throughout the device. This information plus the use of one-dimensional steady-flow relations allows one to calculate the mass flow through the device. Then, knowing the mass flow, the total pressure can be calculated at each pressure measurement location by using the average of the measured static pressures. From this information, the total pressure losses associated with various elements of the test device can be computed.

The results of this exercise are presented in Table 1. According to the results shown, about 1.3% of the total pressure at the inlet is lost between the inlet and the stator stage. About 3.9% of the total pressure of the flow entering the stator is lost in the stator stage. The largest loss shown occurs across the turning vanes where about 10% of the total pressure of the flow entering the turning vanes is lost. The combined loss across the stator and turning vanes is about 14% of the total pressure existing immediately upstream of the stator. An additional loss of 4.9% of the total pressure of the flow leaving the turning vanes occurs between the turning vanes and a point just upstream of the orifice plate. Overall, about 19% of the total pressure at the inlet is lost as the flow travels through the test device.

Estimates of the losses occurring in the stator and turning vanes have been computed using the methodology given by Balje [22] and are also presented in Table 1 for comparison of the experimental results. Two types of losses must be considered: profile losses and end wall losses. For profile losses, Balje's method provides an estimate of the minimum loss expected for an optimum cascade. The pertinent aerodynamic and geometric parameters for the stator stage have been provided by Garrett AiResearch and are listed in Table 2. In computing the losses for this stage, the root and tip Zwiuffel coefficients were averaged and Balje's formulae used. It is noteworthy that the average chord pitch ratio determined for the stator stage using the parameters given in Table 2 agrees very well with that obtained using the average Zwiuffel coefficient in the expression for the optimum chord pitch ratio recommended in Balje's paper. According to his method, the minimum profile total pressure loss expected across the stator stage is about 0.8%.

The profile loss for the turning vanes has been computed in a similar fashion. However, the turning vanes in this experiment were not optimized, and therefore one should expect losses larger than that given by the method of Reference 22. In computing the profile losses, the geometric data shown in Table 3 were used, and the Zwiuffel coefficient was assumed to be 0.9--the optimum value, according to Balje. As shown in Table 1, the resulting minimum predicted total pressure profile loss for the turning vanes is about 13%, much larger than that for the stator stage.

In Reference 22, two methods are presented for computing minimum end wall losses. One method is based on the premise that the end wall loss is proportional to the profile loss and the ratio of wetted areas of the end wall and blade surfaces. This method results in the uppermost end wall loss value tabulated in Table 1. The results shown indicate that the end wall total pressure losses predicted by this method are quite small, being about 0.3% and 0.7% for the stator and turning vanes, respectively.

However, as Balje points out, this method does not properly account for the influence of initial boundary-layer thickness. The second method he gives

does account for this effect through a correction factor which is applied to a formula given for zero initial boundary-layer thickness. The correction factor depends on the ratio of initial boundary-layer thickness to cascade blade height, starting at 1 for a value of 0 for this ratio and approaching 3 for values of this ratio exceeding about 0.03. In the present case, a correction factor equal to 3 is appropriate. In that case, the end wall losses are the lowermost values shown in Table 1.

By comparing the losses obtained from both methods for the stator, it is apparent that the method that accounts for initial boundary-layer thickness predicts a much higher end wall loss than does the other method. Furthermore, since the predicted end wall and profile losses are comparable for the stator, the overall loss, which is taken to be the superposition of the end wall and profile losses, is strongly affected by the choice of method used to determine the end wall loss. Depending on the methodology used, the resulting minimum overall predicted loss for the stator is about 1.1% and 1.8%, as shown in Table 1. This comparable experimental value is shown to be about 3.9%, which is reasonably consistent with the predictions.

In the case of the turning vanes, the two methods for predicting end wall losses are more nearly equivalent than is the case for the stator. Furthermore, the profile loss for the turning vanes is so large in comparison to the end wall loss that the difference in overall combined loss is not significantly affected by the choice of end wall loss prediction method. In both cases, the combined minimum total pressure loss is about 14%. Surprisingly, this is somewhat larger than the experimental value of 10%. It should be recalled that the turning vanes were not optimized, and therefore one would expect that the experimental losses would be significantly larger than the minimum predicted for an optimized cascade. However, inspection of the comparisons between Balje's predictions and cascade loss data presented in Reference 22 suggests the difference observed here may not be unreasonable after all.

Although differences appear between the data and the predictions for the stator and turning vanes, the overall loss values agree quite well. For

example, the measured total pressure loss across the stator/turning vane combination is about 14%, while the minimum predicted loss is either 14.6% or 15.2%, depending on the method chosen for predicting the end wall losses (see Table 1).

It is to be emphasized that the purpose of the foregoing discussion was to illustrate that the experimental apparatus was performing as anticipated. In addition, some effort was devoted to a first preliminary look at the use of the present test device as a means of investigating cascade losses. The primary aim of the experiments performed to date has been to obtain heat-transfer data. However, the fact that the cascade losses obtained experimentally are reasonably close to predicted values suggests that useful cascade loss data can be obtained, especially once improvements are made to the present instrumentation.

#### C. VALIDITY OF TRANSIENT HEAT-TRANSFER MEASUREMENTS FOR CURRENT EXPERIMENTS

The results presented by Vidal [18] were utilized<sup>\*</sup> to ascertain that valid transient heat-transfer measurements were obtained for the experimental apparatus and gasdynamic conditions used here. It can be shown by analyzing the thermal response of a metallic sensor mounted on an insulating substrate that the effects of the metallic sensor (0.1 micron thick) can be neglected after about  $10^{-8}$  seconds.

The material presented by Vidal [18] also forms a basis for establishing the minimum substrate thicknesses that can be regarded as semi-infinite, or equivalently, the maximum test time that will yield data that can be interpreted with the one-dimensional transient heat-conduction equation. This question can be resolved using Eq. 18 in Ref. 18, specialized to a homogeneous substrate material,  $\sigma = 0$ . The resulting relation is differentiated to determine the heat transferred at any depth in the substrate, and this is compared with the heat

---

<sup>\*</sup>The authors are indebted to R. J. Vidal for helpful suggestions in the performance of this analysis.

entering the substrate at  $y = 0$ . The resulting criterion is

$$\frac{-k \frac{\partial T}{\partial y}}{q} = \operatorname{erfc} \frac{y}{2\sqrt{Kt}} \quad (1)$$

and if it is required that the maximum heat loss out of the back face of the insulator be 10% of the incident heat, the criterion is that the minimum depth of the substrate be  $l_{\min} > 3.644 \sqrt{Kt}$ . For a pyrex substrate and a test time of 20 milliseconds, the value of  $l_{\min}$  was found to be  $4 \times 10^{-4}$  meters (0.016 inches). The pyrex substrate used in the present experiments was  $7.11 \times 10^{-4}$  meters (0.028 inches) thick which fulfills this requirement. From the results presented in Ref. 18 and the above discussion, it can be seen that  $l_{\min}$  will increase with increasing test time. It follows from Eq. (1) that transient heat-transfer measurements are subject to the least uncertainty if the test time is sufficiently short to insure that the characteristic penetration depth,  $2\sqrt{Kt}$ , is small by comparison with the thickness of the substrate. For the experimental conditions (test time on the order of 20 milliseconds) used herein, the characteristic penetration depth was approximately  $2.23 \times 10^{-4}$  meters (0.00088 inches) for a substrate thickness of  $7.11 \times 10^{-4}$  meters (0.028 inches).

A strong motivation for using thin-film techniques and transient test techniques is that one can minimize the characteristic penetration depth,  $2\sqrt{Kt}$ , and thereby be assured that the effects of axial heat conduction are confined to a thin layer at the surface and that these effects will be small. An approximate criterion for evaluating the magnitude of the axial heat conduction effects can also be obtained from Eq. 19 of Ref. 18 if it is assumed that the axial, or transverse heat transfer is in laminae and is not influenced by the temperature gradients along the coordinate normal to the surface. The resulting criterion cannot be regarded as quantitatively rigorous, but rather it serves as a qualitative indicator of the severity of the problem. Equation 18 from Ref. 18 is cast into the following form

$$T(y, t, x) = q(x) \left\{ 2 \sqrt{\frac{t}{\pi k \rho c}} e^{-\frac{y^2}{4Kt}} - \frac{y}{k} \operatorname{erfc} \frac{y}{2\sqrt{Kt}} \right\} \quad (2)$$

and the axial heat transfer,  $q_a(y, t) = -k \frac{\partial T}{\partial x}$ , is compared with the heat transfer to the surface,  $q(x)$ . The following relation is obtained.

$$\frac{q_a(y, t)}{q(x)} = -\frac{1}{\sqrt{\pi}} \frac{2\sqrt{KT}}{q(x)} \frac{dq}{dx} \left\{ e^{-\frac{y^2}{4Kt}} - \sqrt{\pi} \frac{y}{2\sqrt{Kt}} \operatorname{erfc} \frac{y}{2\sqrt{Kt}} \right\} \quad (3)$$

It should be noted that the term in the bracket is identically the ratio of the temperature at the depth,  $y$ , to the surface temperature, and the axial heat transfer can be minimized by minimizing the characteristic penetration depth,  $2\sqrt{KT}$ , or by maximizing the characteristic heat-transfer gradient,  $q/2\sqrt{KT}$ , in comparison with the physical gradient  $dq/dx$ .

Equation (3) has been evaluated for shock-tunnel test times of 20 milliseconds, for a pyrex substrate, and for typical maximum and minimum heat transfer gradients  $\frac{1}{q}(dq/dx) = 1.06$  to  $0.138$  1/cm. The results are tabulated in Table 4 for depths equal to the characteristic penetration depth, 0.04 cm, and at depths of 1.10, 1/20, and 1/100 of the characteristic depth. It can be seen that the most severe axial losses are confined to a layer of the surface which is about  $8 \times 10^{-3}$  cm thick, or 20% of the characteristic penetration depth. A typical sensor diameter of interest to turbine blade investigations is about 0.10 cm, or about 10 times larger than the layer in which the losses are greatest. Consequently, the actual maximum losses, the product of the heat-transfer rate and the area, are about 0.1% or less.

For the experiments reported herein, it was found that both the back-face losses and the transverse losses were negligible and that the data could be interpreted with the existing one-dimensional analysis with a high level of confidence.

#### D. PRESENTATION OF HEAT-TRANSFER RESULTS

An experimental program demonstrating the feasibility of the technique described herein for obtaining detailed spatial distributions of heat-transfer rate on full-scale engine components has been completed. The reflected-shock

reservoir conditions in the equilibrium interface region were a pressure of  $1.51 \times 10^7$  newtons/m<sup>2</sup> at a reflected-shock temperature of 1570°K. Using one-dimensional calculation techniques, the known area of the aft diffuser and orifice plate, and the measured static pressure, one can calculate the Mach number in the aft diffuser and the mass flow rate. The results of this calculation give a Mach number in the aft portion of approximately 0.24 and a mass flow rate of 3.50 Kgm/sec for the 176° sector or 7.17 Kgm/sec for the full turbine. Knowing the forward area and the mass flow rate, an iteration technique was used to find the Mach number in the forward section ahead of the stator to be 0.15 at a total pressure of  $8.74 \times 10^5$  newtons/m<sup>2</sup> giving a flow velocity of about 114 m/sec and a gas density of 1.92 Kgm/m<sup>3</sup>. The resulting Reynolds number ahead of the stator was  $4.27 \times 10^6$  per meter or approximately  $1.3 \times 10^5$  based on mid annular chord length. The Mach number at the stator exit tip was calculated to be approximately 0.7 based on the average static pressure at locations (14), (15), and (16), and based on the total pressure ahead of the stator inlet. The stator stage was designed for a Mach number of 0.8 at this location and a mass flow rate approximately 13.61 Kgm/sec for the entire turbine or 6.65 Kgm/sec for the 176° sector. Therefore, the mass flow rate used in these experiments was approximately half of the design condition. In subsequent experiments, the mass flow will be increased to the appropriate value by simply increasing the shock-tunnel primary nozzle throat area which has the effect of moving the inlet to the location in the primary nozzle where the Mach number is equal to 4.0. For the experiments reported here, the Mach number at the entrance to the inlet was approximately 4.5 and the post-shock specific heat ratio was approximately 1.3. The design Mach number of 0.8 at the stator exit tip can be achieved by increasing the orifice size which also will increase the mass flow rate.

Detailed heat-transfer rate measurements were obtained from the thin-film gages by processing the gage output voltage through a standard heat-flux network developed by Skinner [23]. Prior to initiating the experiments, each of the gages was calibrated at 297.6°K, 313.8°K and 334.5°K using a temperature-controlled oil bath. The temperature coefficient of resistance determined in this manner is used in obtaining the calibration signal (shown on the oscilloscope data records discussed later in this section) determined for each gage prior to

every run. The room temperature resistance of each gage was measured prior to an experiment and if a change in resistance was observed, then the calibration signal could be appropriately compensated. However, during the course of the experimental program reported here, the room temperature resistance of the individual gages remained essentially unchanged.

Figures 14-17 present the detailed locations of the heat-transfer gages on the hub end wall, tip end wall, airfoil suction surface and the airfoil pressure surface. The solid dot represents the location of the heat-transfer gage on the projected surface and the number in the circle represents the heat-transfer gage number. The coordinate system for location of the gage on the surface is shown on each figure and the coordinates are tabulated in Table 5 along with the heat-transfer rates. The only coordinate requiring explanation is the X-coordinate used for the end wall location. The X-distance is measured along the ray shown drawn through the points. The location of heat-transfer gages 29-52 on the tip end wall and gages 1 to 16 on the airfoil pressure surface can be seen clearly on the photographs of the end wall shown in Figs. 7 and 8. The hub end wall gages 58 to 63 can be seen in Fig. 9.

Figures 18 and 19 are typical of the heat-transfer rate measurements obtained in these experiments. The calibration signal discussed above is shown on the left side of the data record of both figures for each gage. The data presented in Fig. 18 were obtained from heat-transfer gages located on the pressure side of the airfoil. Referring to Fig. 7 gage #3 is the centerline gage located nearest the leading edge and gage #11 is the third gage on the centerline. Figure 19 presents data obtained from gage #54 (upper channel) which was located on the hub wall which can be seen on Fig 9, and the data from gage #30 (lower channel) which is the center gage on the top row of end wall gages as seen on Fig. 7. The significant point to be noted from these figures is that even though the characteristic of the data records during the early-time flow-establishment period is different depending upon where the gage is located, in all cases uniform flow is achieved at approximately the same time and the heat-transfer rate remains relatively uniform during the useful test time. The useful test time is noted on Figs. 18 and 19 and shown to be about 12 milliseconds.

The time period of approximately 8 milliseconds preceding the test time is the flow establishment time discussed in Ref. 14. The heat-transfer rates to be determined from these records were read at relatively late times and the surface temperature had increased above room temperature. Consequently, it was necessary to incorporate a correction for the temperature variation of the  $\rho c k$  product of the pyrex substrate. This correction results in an increase of approximately 10 percent over the values taken from the oscilloscope records.

Figures 20-23 present a summary of the heat-transfer rate measurements for the end wall, hub wall, pressure side of airfoil and suction side of the airfoil. Once again, the solid dot represents the location of the heat-transfer gage on the projected surface, the number in the circle is the gage number referred to in Table 4 and the number under the dot is the heat-transfer rate in  $\text{joules/m}^2 \text{ sec}$  obtained by averaging the results of three separate experiments. The reproducibility of the experimentally determined heat-transfer rate at a given location was in general within  $\pm 5\%$  for the experiments performed.

In interpreting the heat-transfer results presented in Figs. 20-23, it should be recalled that the total pressure and mass flow rate are approximately 50% of the design values for the stator. The total temperature and Mach number distribution are near design values. Because of the lower total pressure, the heat-transfer rates will be lower than would be expected under actual engine operating conditions. However, for the purposes of using these experimental heat-transfer results to verify calculation techniques, the deficiency in pressure and mass flow should not present a problem since the inlet gasdynamic conditions are known.

The results for the end-wall heat-transfer rate measurements are presented in Fig. 20. A local hot spot can be seen near the leading edge on the suction side of the airfoil. The heat-transfer rate values from about mid-chord to the trailing edge are significantly elevated over the entrance region values consistent with what was observed by Blair [6].

The hub wall results are presented in Fig. 21. It can be observed that the measured heat-transfer rates for this surface are fairly uniform with the exception of those measurements taken in the vicinity of the suction side of the airfoil. Of these later measurements, the one nearest the leading edge was greater than the near mid-chord value. Unfortunately, heat-transfer gage #58, which would have provided a more complete profile, was damaged during installation and did not operate.

Results of the heat-transfer measurements obtained on the airfoil pressure surface are shown in Fig. 22. The gages at the near centerline location illustrate a trend starting with gage #3 of first decreasing then increasing to a much higher value at gage #16. Near the end and hub walls, the heat-transfer rate is relatively uniform with the exception of a local hot spot at gages #4 and #5.

Figure 23 presents the results obtained for the suction side of the airfoil. Near the hub wall, gages #17, #18, and #22, the heat-transfer rates are as large or larger than those experienced on the trailing portion of the end wall. In addition, gages #25 to #28 on the near centerline of this surface also indicated relatively large heat-transfer rates. By comparison, the heat-transfer values obtained near the end wall were significantly lower and of the order of those measured on the pressure side of the airfoil.

Detailed interpretation of the results presented in Figs. 20-23 in terms of local vortices or other flow disturbances has not yet been completed. However, a detailed comparison has been presented by Dodge [24] between his predicted heat-transfer rates and the measurements reported herein. Relatively good agreement is demonstrated between the predicted and measured values for the stator tip and hub end walls. The distributions on the pressure and suction surface of the airfoil are in good agreement but the predicted heat-transfer levels are greater than the measured values. Dodge attributes these higher predicted values to the nontransitioning turbulence model used in his calculation.

## SECTION V

### CONCLUSIONS AND RECOMMENDATIONS

The application of state-of-the-art shock-tube technology and well established transient-test techniques results in accurate measurement of the spatial distribution of heat-transfer rate on the first stage stationary inlet nozzle of the AiResearch TFE-731-2 engine under gas-dynamic conditions that simulate engine operating conditions. The test time and mass flow rate available from the shock-tube reservoir and the flow establishment time in the test section are all acceptable for the purposes of performing these heat-transfer rate measurements. In addition, it appears that useful cascade loss data can be obtained using the experimental apparatus discussed herein.

Additional heat-transfer data at greater mass flow rates and over a range of Reynolds number would provide a much needed data base for comparison with the results of predictive models. These measurements would also provide "no-rotor data" that could be used at a later date to ascertain the upstream influence of the rotor. It would be of interest to initiate experimental studies of the influence of mass injection on heat-transfer rates for the three-dimensional flow field associated with the stator nozzles. Perhaps the most ambitious extension of the research program discussed in this report would be to go directly to the introduction of an instrumented rotor and measure heat-transfer rates on one of the rotor blades simultaneous with stator measurements similar to those discussed herein.

Table 1  
TABULATION OF PREDICTED AND MEASURED LOSSES

	INLET TO STATOR	STATOR	TURNING VANES	STATOR + TURNING VANES	TAILPIPE	OVERALL
$\left(\frac{\Delta P_t}{P_t}\right)$ MEAS	-0.0132	-0.0393	-0.1007	-0.1400	-0.0492	-0.1894
$\left(\frac{\Delta P_t}{P_t}\right)^*$ PRED. MIN.	-	-0.0110 -0.0178	-0.1353 -0.1339	-0.1463 -0.1517	-	-
$\left(\frac{\Delta P_t}{P_t}\right)$ PRED. MIN. PROFILE		-0.0799	-0.1283			
$\left(\frac{\Delta P_t}{P_t}\right)^*$ PRED. MIN. ENDWALL		-0.00301 -0.00987	-0.0070 -0.0056			
$\left(\frac{\Delta P_t}{P_t}\right)^*$ PRED. MIN. ENDWALL + PROFILE		-0.0110 -0.0178	-0.1353 -0.1339			

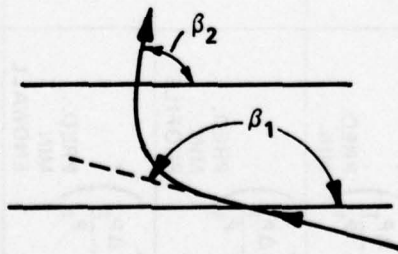
NOTE: \* SEE TEXT FOR SIGNIFICANCE OF TWO ROWS OF NUMBERS  
SHOWN IN THESE COLUMNS

Table 2  
STATOR VANE DATA

	HUB	TIP
DESIGN RADIUS, METERS (IN)	0.10986(4.325)	0.14072(5.540)
INLET FLOW ANGLE, DEG	0.000	0.000
EXIT FLOW ANGLE, DEG	70.246	67.516
ψ 5798, ZWEIFEL LOADING COEFF.	0.6750	0.7030
LEADING EDGE THICKNESS, METERS (IN)	0.001067(0.042)	0.001321(0.052)
TRAILING EDGE THICKNESS, METERS (IN)	0.000508(0.020)	0.000508(0.020)
THROAT DIMENSION, METERS (IN)	0.00571(0.2248)	0.00824(0.3246)
C <sub>X</sub> , AXIAL CHORD, METERS (IN)	0.01712 (0.6740)	0.02276 (0.8959)
C <sub>X</sub> /S, AXIAL SOLIDITY	1.0169	1.0552
EXIT BLADE ANGLE, DEG	68.327	66.0560
ASPECT RATIO, VANE HEIGHT/C <sub>X</sub> MEAN	1.5500	
TRAILING EDGE BLOCKAGE, %	8.17	5.80

Table 3  
SUMMARY OF PHYSICAL PARAMETERS OF TURNING VANES

BLADE HEIGHT, METERS (IN)	0.03099(1.22)
BLADE CHORD, METERS (IN)	0.0292(1.148)
CAMBER LINE LENGTH, METERS (IN)	0.03099(1.22)
CIRCUMFERENTIAL BLADE SPACING, METERS (IN)	0.0192(0.756)
FLOW TURNING ANGLE, DEG	70
RADIUS OF TURNING VANES, METERS (IN)	CIRCULAR ARC R = 0.0254(1.0)
β <sub>1</sub> = 160°	
β <sub>2</sub> = 90°	



**Table 4**  
**COMPARISON OF AXIAL HEAT TRANSFER TO SURFACE HEAT TRANSFER**

$y$ (cm)	$\frac{T(y)}{T(o)}$	$\left(\frac{q_a}{q}\right)_{\max}$	$\left(\frac{q_a}{q}\right)_{\min}$
$4 \times 10^{-4}$	0.964	0.011	0.002
$4 \times 10^{-3}$	0.681	0.008	0.001
$8 \times 10^{-3}$	0.441	0.005	0.001
$4 \times 10^{-2}$	0.015	0.0000	0.0000

Table 5  
SUMMARY OF HEAT-TRANSFER RATE DATA AND GAGE LOCATIONS

GAGE #	X INCHES	Y INCHES	RUN A $\dot{q}$ BTU/ft <sup>2</sup> sec	RUN B $\dot{q}$ BTU/ft <sup>2</sup> sec	RUN C $\dot{q}$ BTU/ft <sup>2</sup> sec	(A+B+C)/3 $\dot{q}_{avg}$ BTU/ft <sup>2</sup> sec	GAGE #	X INCHES	Y INCHES	RUN A $\dot{q}$ BTU/ft <sup>2</sup> sec	RUN B $\dot{q}$ BTU/ft <sup>2</sup> sec	RUN C $\dot{q}$ BTU/ft <sup>2</sup> sec	(A+B+C)/3 $\dot{q}_{avg}$ BTU/ft <sup>2</sup> sec
1	1.230	0.104	103	93	108	101	29	0.761	0.121	97	83	97	92
62	1.050	0.092	91	107	107	102	30	0.618	0.121	116	113	106	111
3	0.712	0.109	110	122	124	119	31	0.339	0.121	142	154	154	150
4	0.303	0.105	-	112	130	121	32	0.591	0.197	183	169	154	169
5	0.122	0.096	132	132	140	135	33	0.446	0.239	165	202	201	189
6	0.702	0.209	-NG-	-NG-	-NG-	-NG-	34	0.300	0.285	129	139	129	132
7	0.302	0.196	84	91	91	89	35	0.152	0.330	82	94	89	88
8	0.129	0.190	98	104	96	99	36	0.084	0.369	104	108	102	105
9	1.145	0.295	85	85	74	81	37	0.095	0.254	117	141	124	127
10	0.961	0.273	87	89	87	88	38	0.371	0.379	151	157	133	147
11	0.678	0.309	86	90	94	90	39	0.241	0.492	127	146	140	138
12	0.296	0.301	97	93	97	96	60	0.115	0.582	141	153	141	145
13	0.122	0.291	-NG-	-NG-	-NG-	-NG-	41	0.267	0.547	190	186	190	188
14	0.683	0.409	84	76	115	92	42	0.122	0.582	177	165	161	168
15	0.683	0.509	116	111	126	117	43	0.434	0.684	175	193	193	187
16	0.642	0.609	144	134	134	137	44	0.125	0.684	149	169	169	162
17	0.135	0.146	222	236	236	231	45	0.283	0.809	169	178	188	176
18	0.305	0.147	252	269	269	263	46	0.125	0.901	176	184	188	176
19	0.720	0.149	162	153	146	154	47	0.075*	0.899	187	186	189	188
20	0.976	0.164	124	113	101	113	48	0.243	1.027	193	193	205	197
61	1.151	0.161	142	131	141	138	49	0.077*	0.967	162	169	175	169
22	0.133	0.228	191	179	145	172	50	0.395	1.034	214	209	219	214
23	0.666	0.236	129	119	124	124	52	0.634	1.036	179	198	185	188
24	1.087	0.247	97	97	89	94	63	0.097	0.132	90	106	100	99
25	0.636	0.334	200	177	181	186	53	0.272	0.125	115	120	114	116
26	0.630	0.414	198	193	179	190	54	0.471	0.125	139	156	151	148
27	0.633	0.494	234	229	221	228	55	0.095	0.314	86	112	109	102
28	0.625	0.579	218	212	190	206	56	0.250	0.314	103	97	91	97
							57	0.421	0.308	132	138	132	134
							58	0.276	0.421	-NG-	-NG-	-NG-	-NG-

NOTE: (1)\* X CO-ORDINATE FOR GAGES 47 AND 49 IS DISTANCE AWAY FROM SUCTION SURFACE  
(2) TO CONVERT INCHES TO METERS MULTIPLY BY 0.0254  
(3) TO CONVERT BTU/ft<sup>2</sup> sec TO JOULES/m<sup>2</sup> sec MULTIPLY BY 97.99  
(4) SEE SKETCHES, FIGS. 14-17 FOR DESCRIPTION OF X AND Y COORDINATES

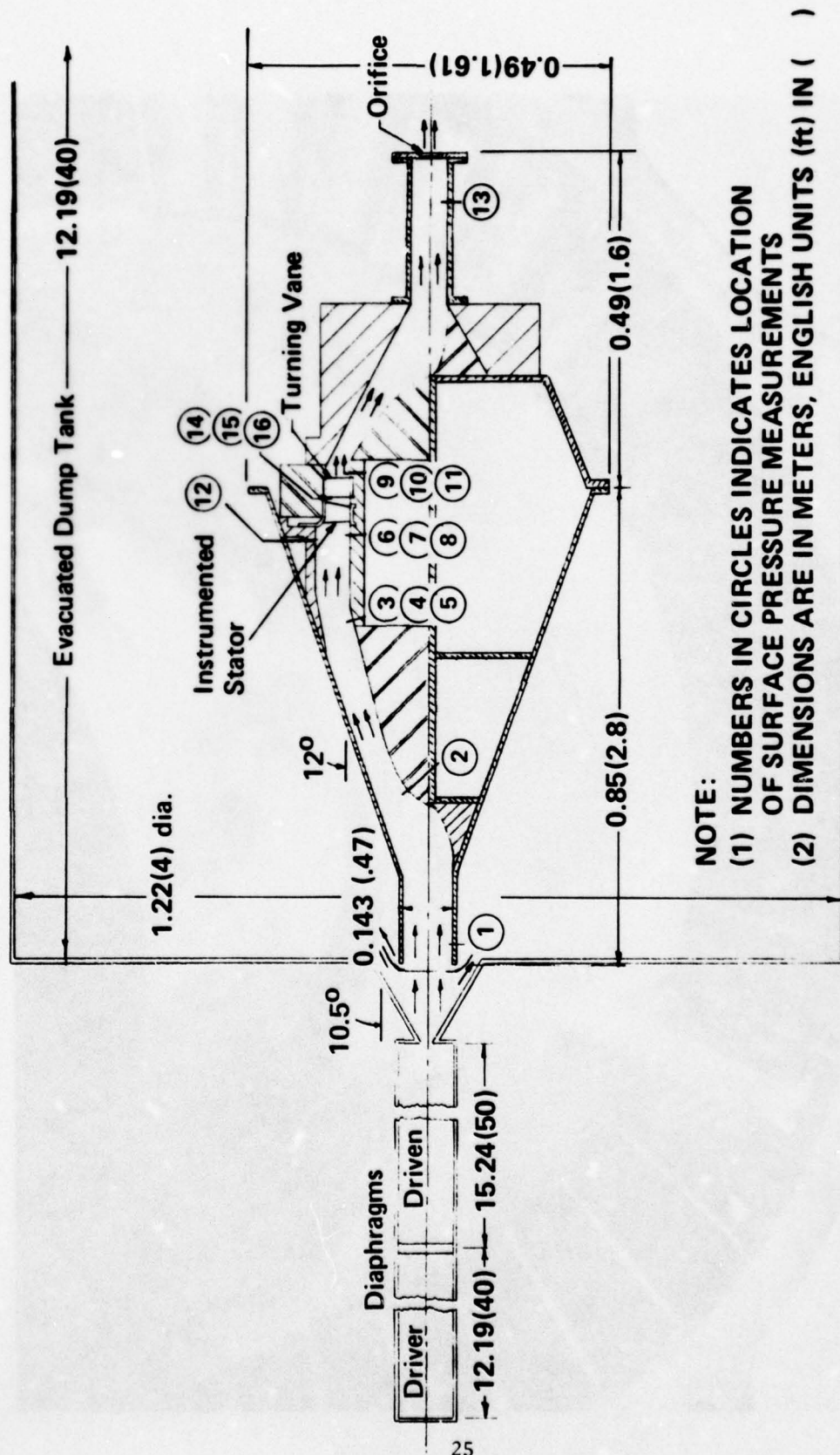


Figure 1 Sketch of experimental apparatus

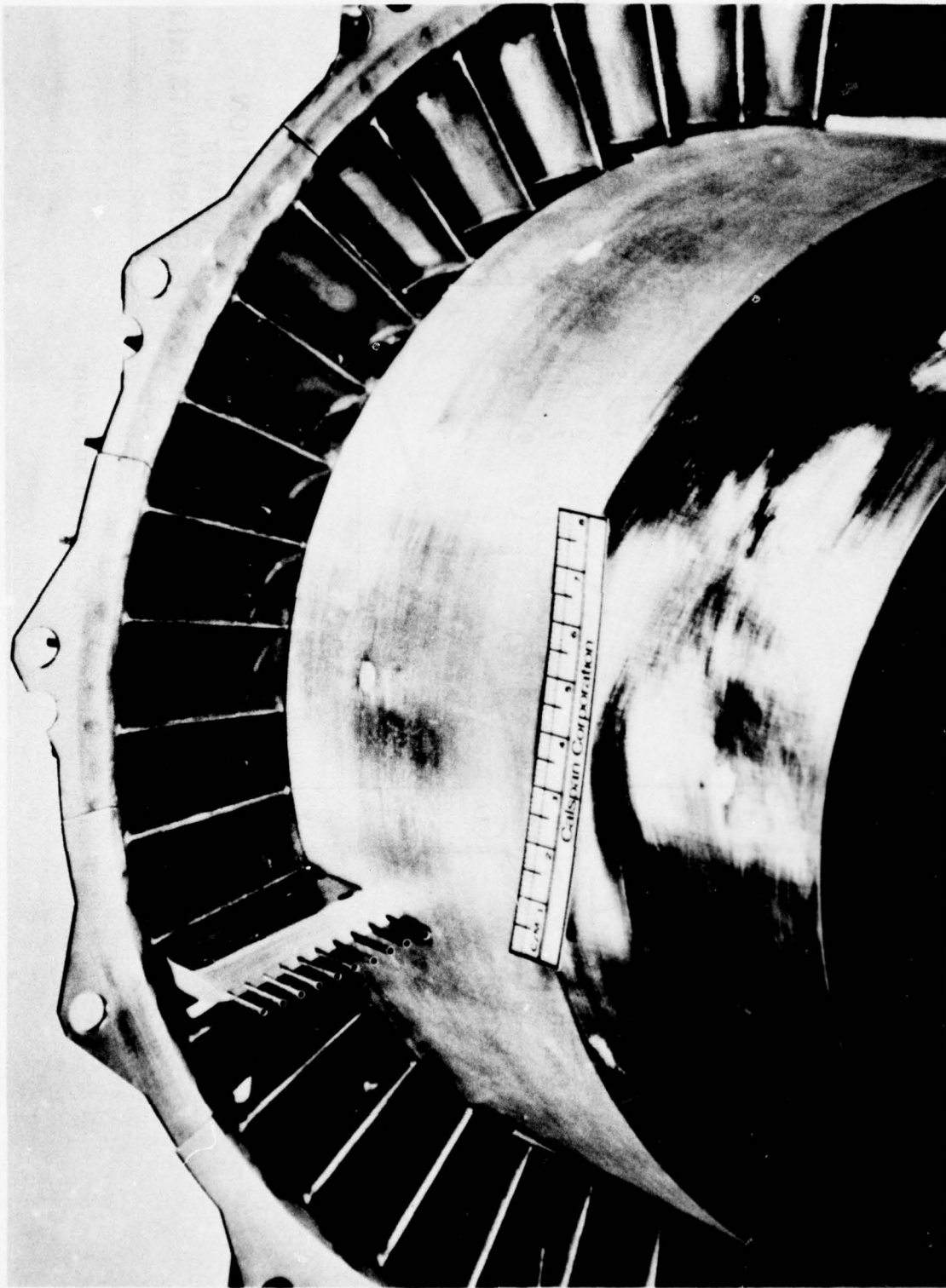


Figure 2 NOZZLE STATOR INSTALLATION IN PORTION OF TEST SECTION

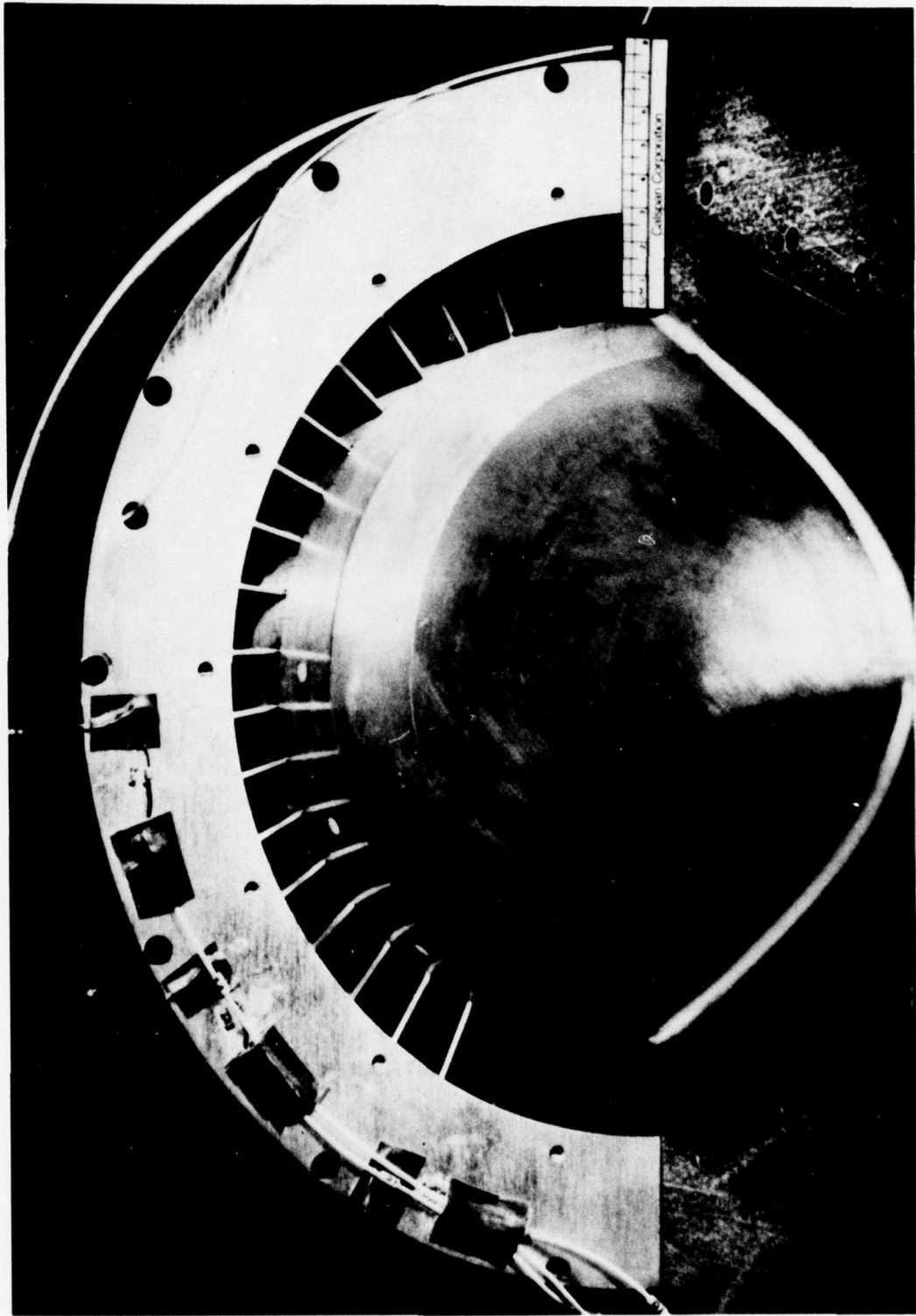
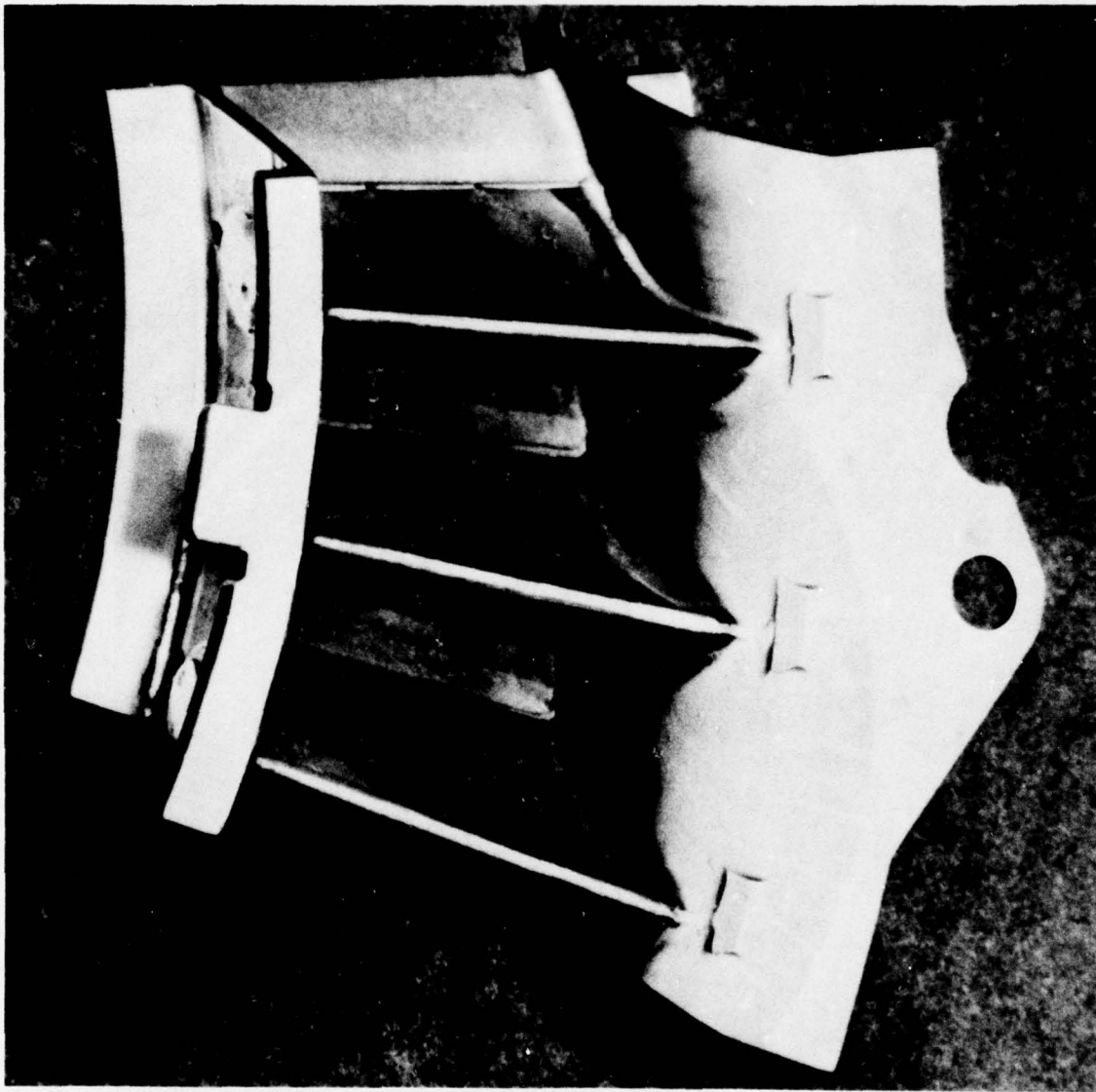


Figure 3 TURNING VANE INSTALLATION IN PORTION OF TEST SECTION



**Figure 4 INLET STATOR PRIOR TO INSTRUMENTATION**

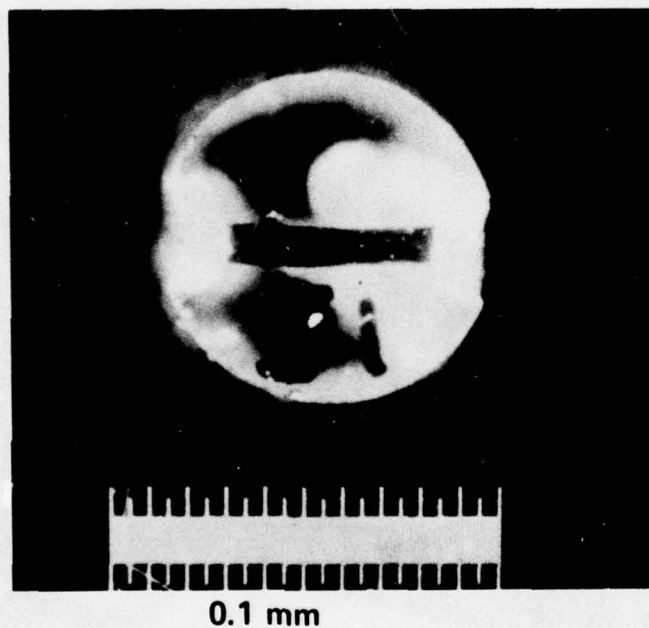


Figure 5 PHOTOGRAPH OF HEAT-TRANSFER GAGE TAKEN THROUGH A LEITZ MICROSCOPE



Figure 6 HOLE LOCATIONS ON AIRFOIL PRESSURE SIDE PRIOR TO INSTALLATION OF HEAT-TRANSFER GAGES



Figure 7 HEAT-TRANSFER GAGES IN TIP ENDWALL AND AIRFOIL PRESSURE SURFACE

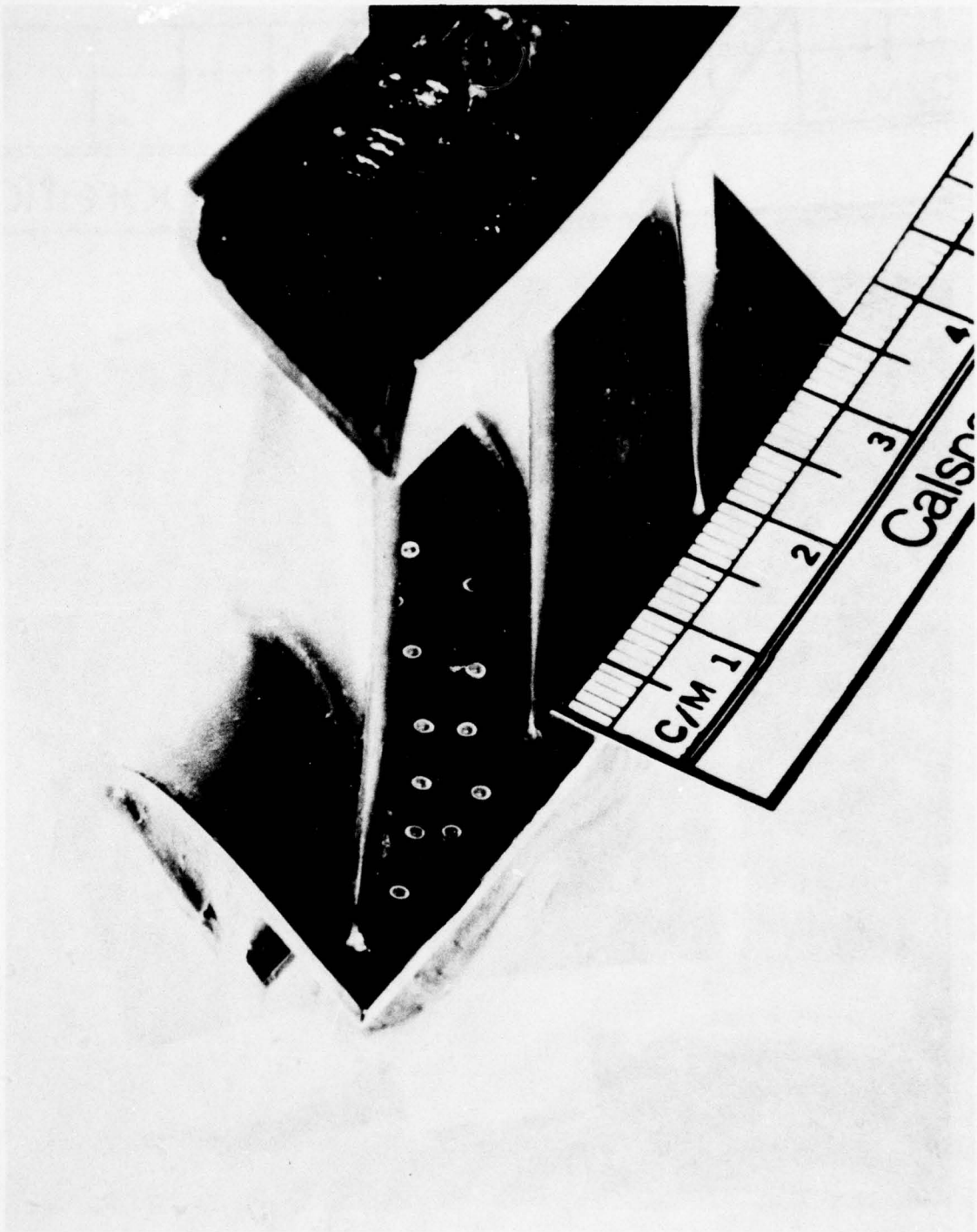


Figure 8 HEAT-TRANSFER GAGES IN TIP ENDWALL

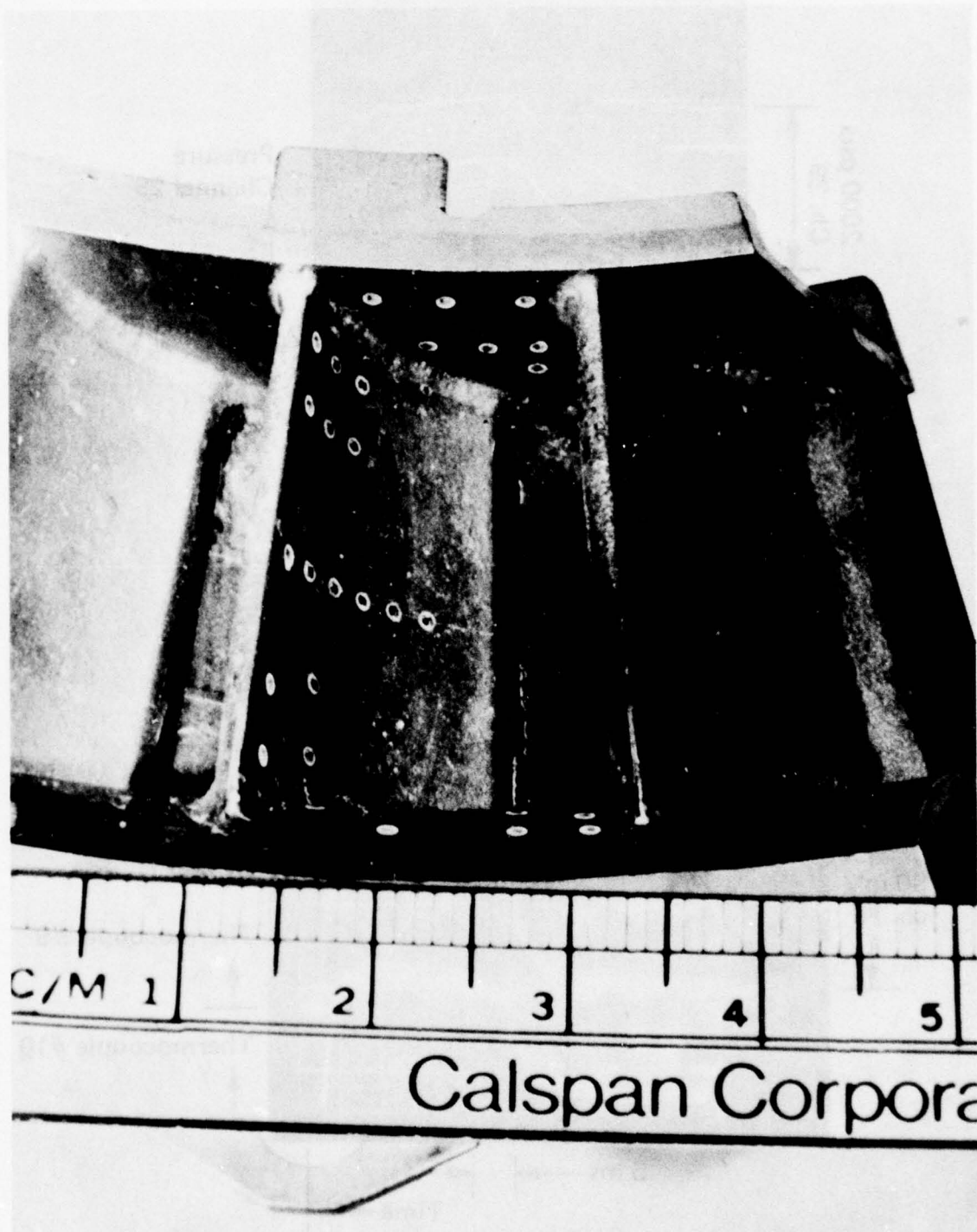


Figure 9 HEAT-TRANSFER GAGES IN HUB ENDWALL

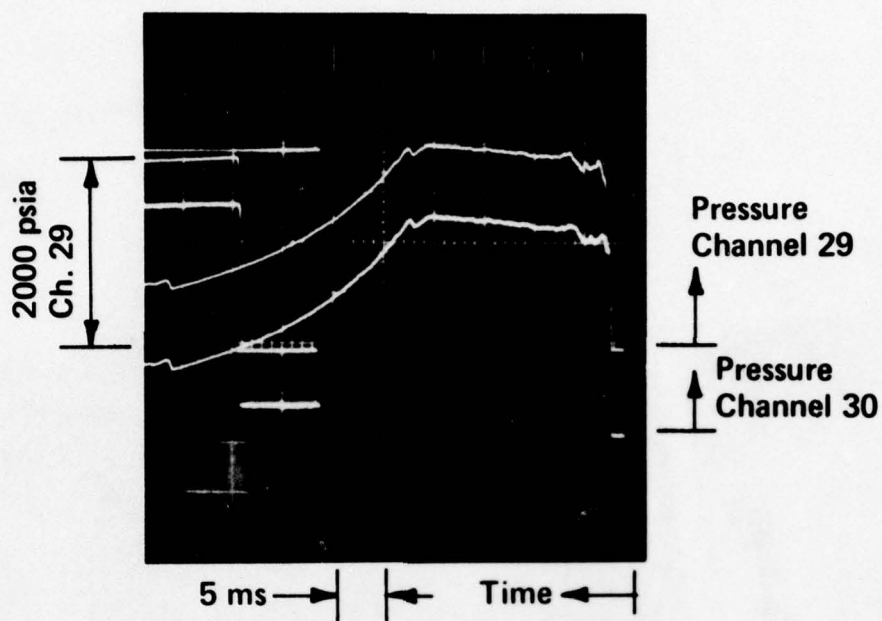


Figure 10 REFLECTED-SHOCK PRESSURE MEASUREMENT

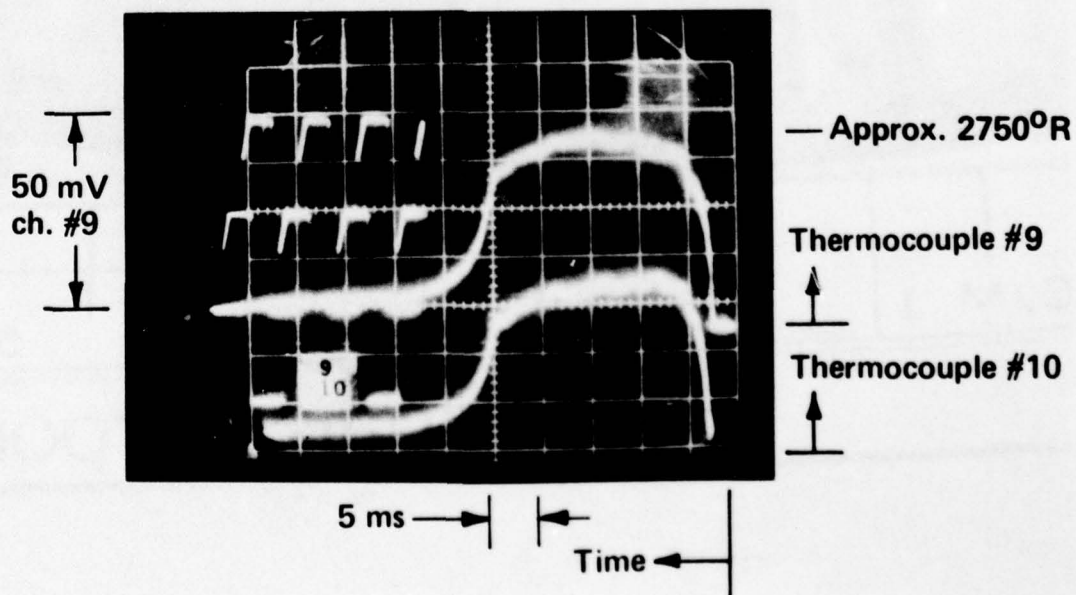


Figure 11 TOTAL TEMPERATURE MEASUREMENTS JUST AHEAD OF STATOR

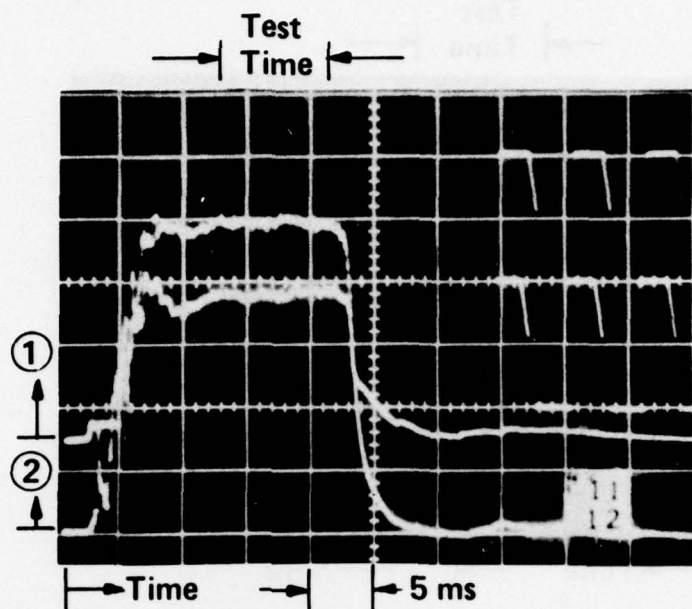


Figure 12 (a) STATIC PRESSURE DATA UPPER CHANNEL: PRESSURE AT ①  
LOCATED AT 2-INCHES FROM INLET LOWER CHANNEL:  
PRESSURE AT ② LOCATED AT 16.6-INCHES FROM INLET

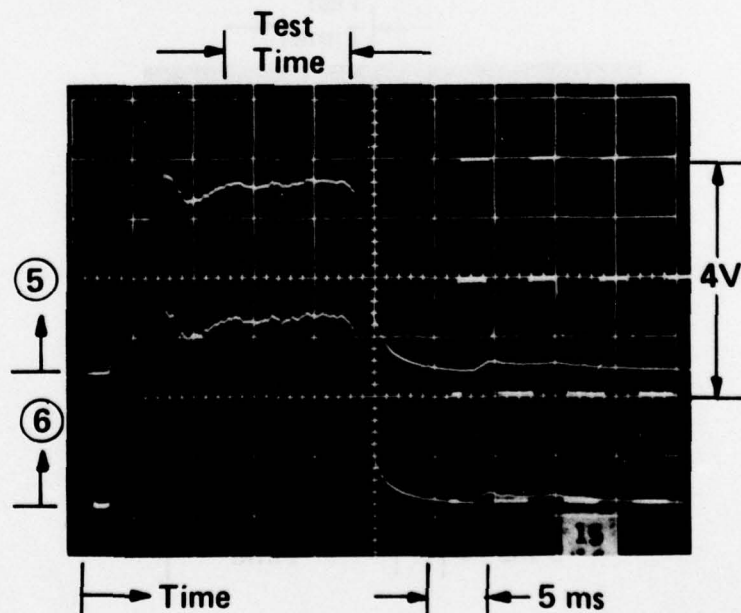


Figure 12(b) STATIC PRESSURE DATA UPPER CHANNEL: PRESSURE AT ⑤  
AT 6-INCHES UPSTREAM OF STATOR LOWER CHANNEL:  
PRESSURE AT ⑥ AT 1.35 INCHES UPSTREAM OF STATOR

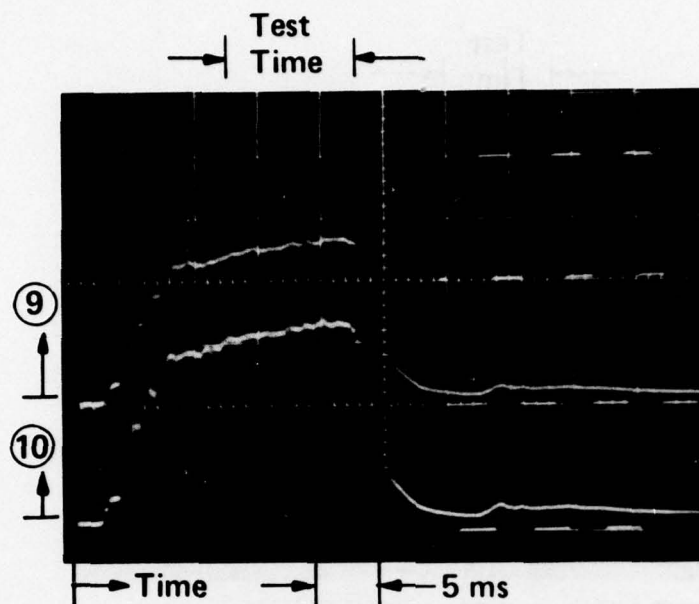


Figure 12(c) **STATIC PRESSURE DATA** UPPER CHANNEL: PRESSURE AT ⑨ LOCATED 0.65-INCHES DOWNSTREAM OF FLOW STRAIGHTENERS LOWER CHANNEL: PRESSURE AT ⑩ LOCATED 0.65-INCHES DOWNSTREAM OF FLOW STRAIGHTENERS

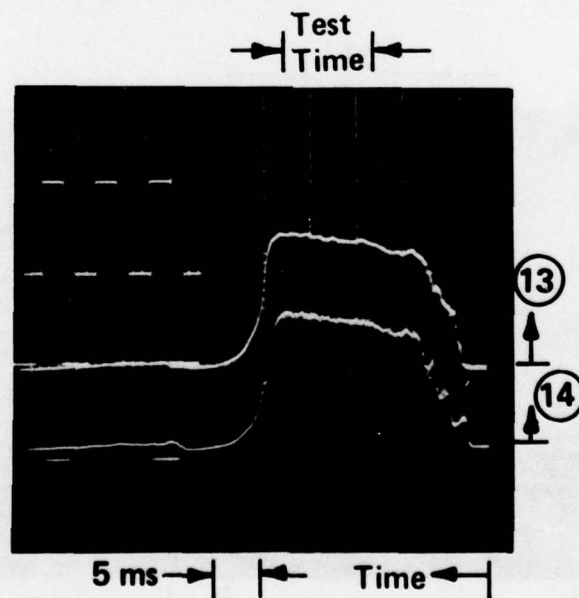


Figure 12(d) **STATIC PRESSURE DATA** UPPER CHANNEL: PRESSURE AT ⑬ LOCATED 4.55-INCHES UPSTREAM OF ORIFICE PLATE LOWER CHANNEL: PRESSURE AT ⑭ LOCATED 0.10-INCHES DOWNSTREAM OF STATOR EXIT PLANE IN TIP WALL

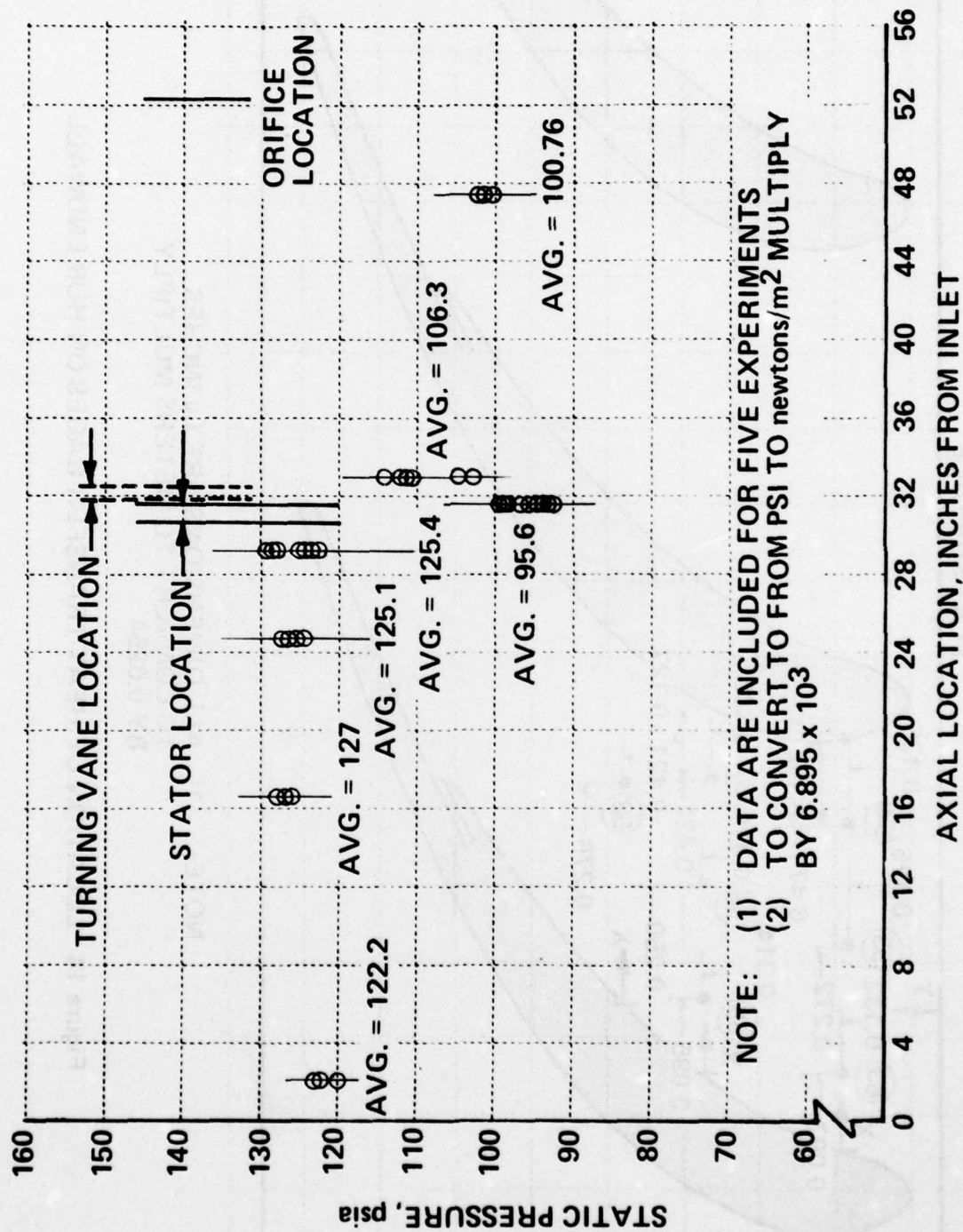


Figure 13 SUMMARY OF STATIC-PRESSURE MEASUREMENTS IN TEST APPARATUS



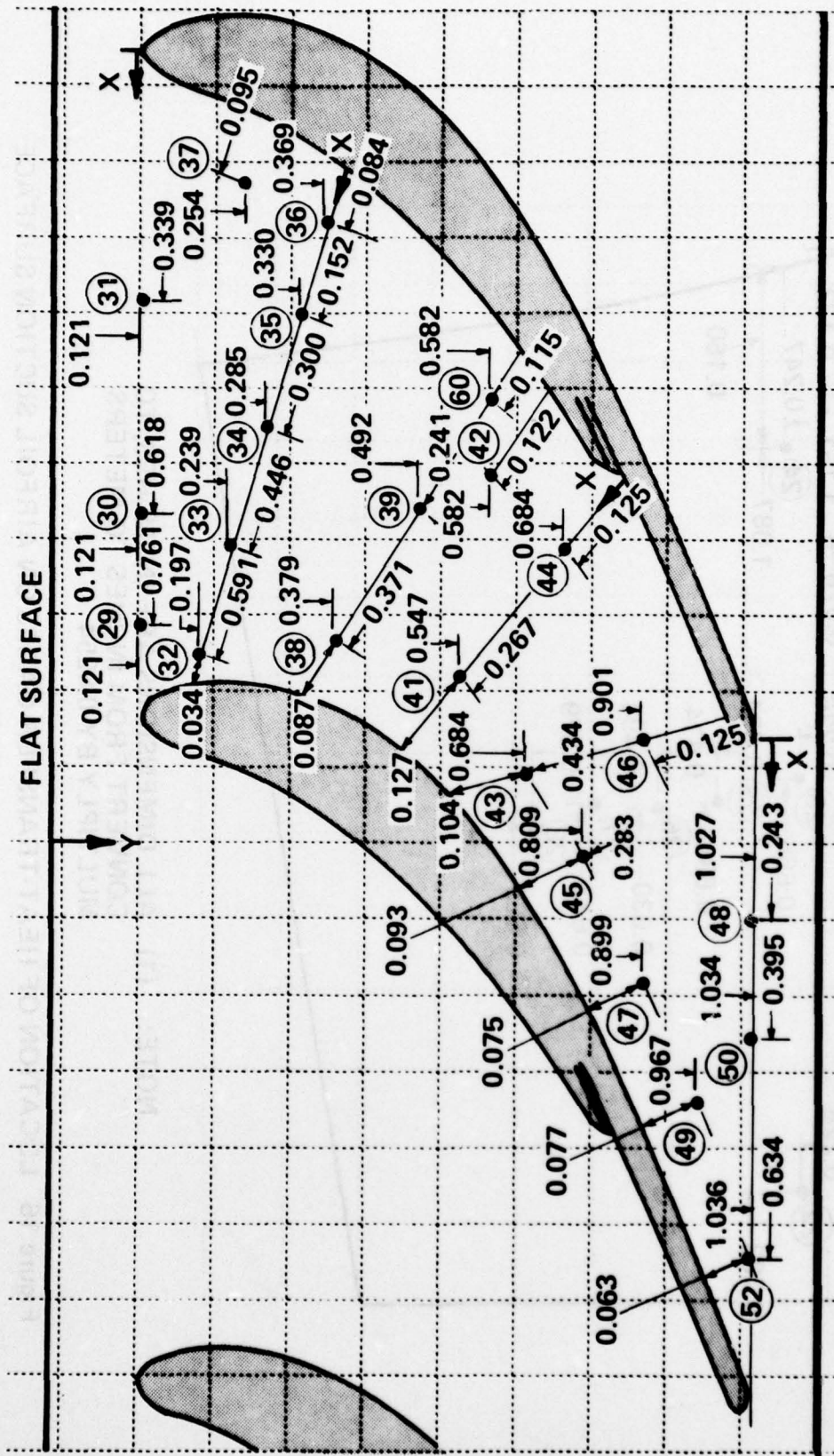
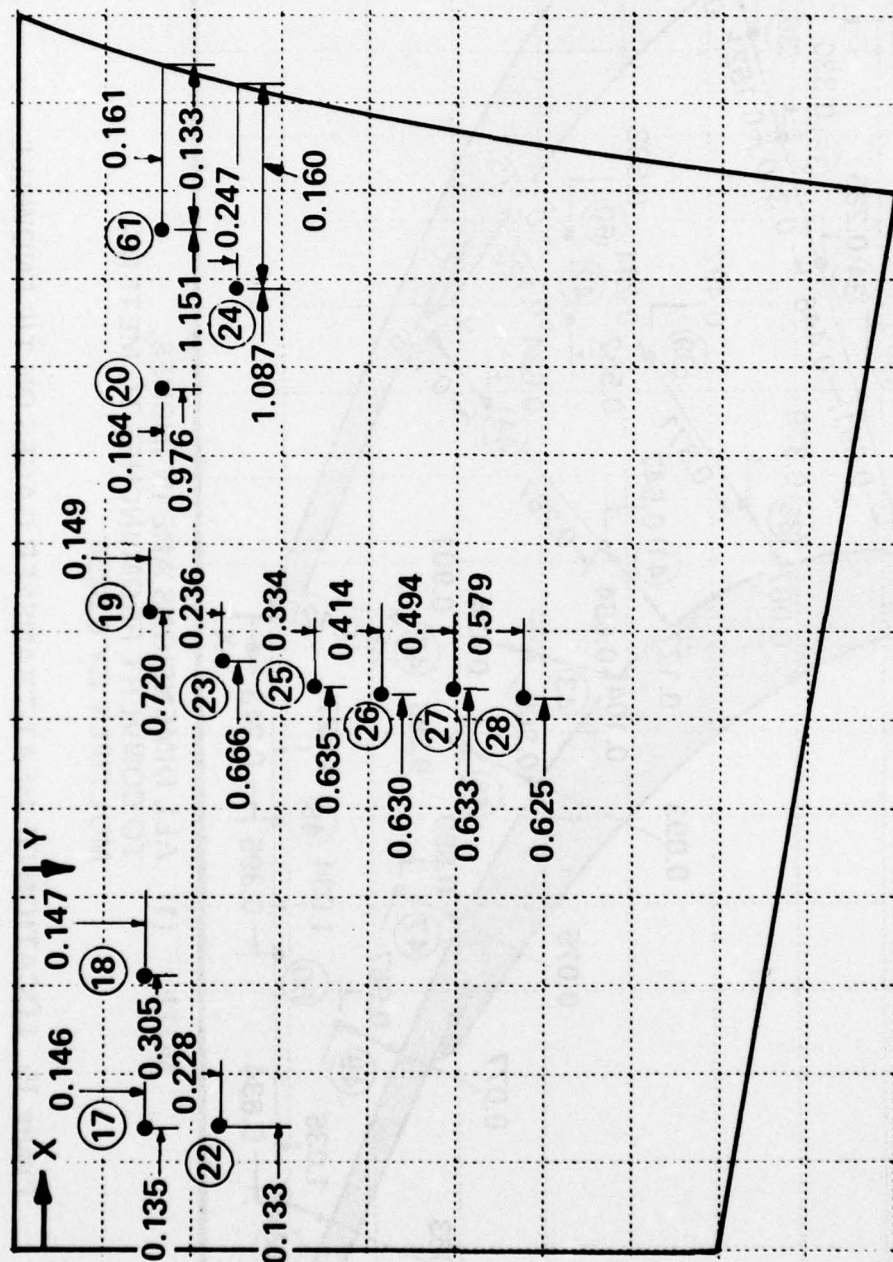
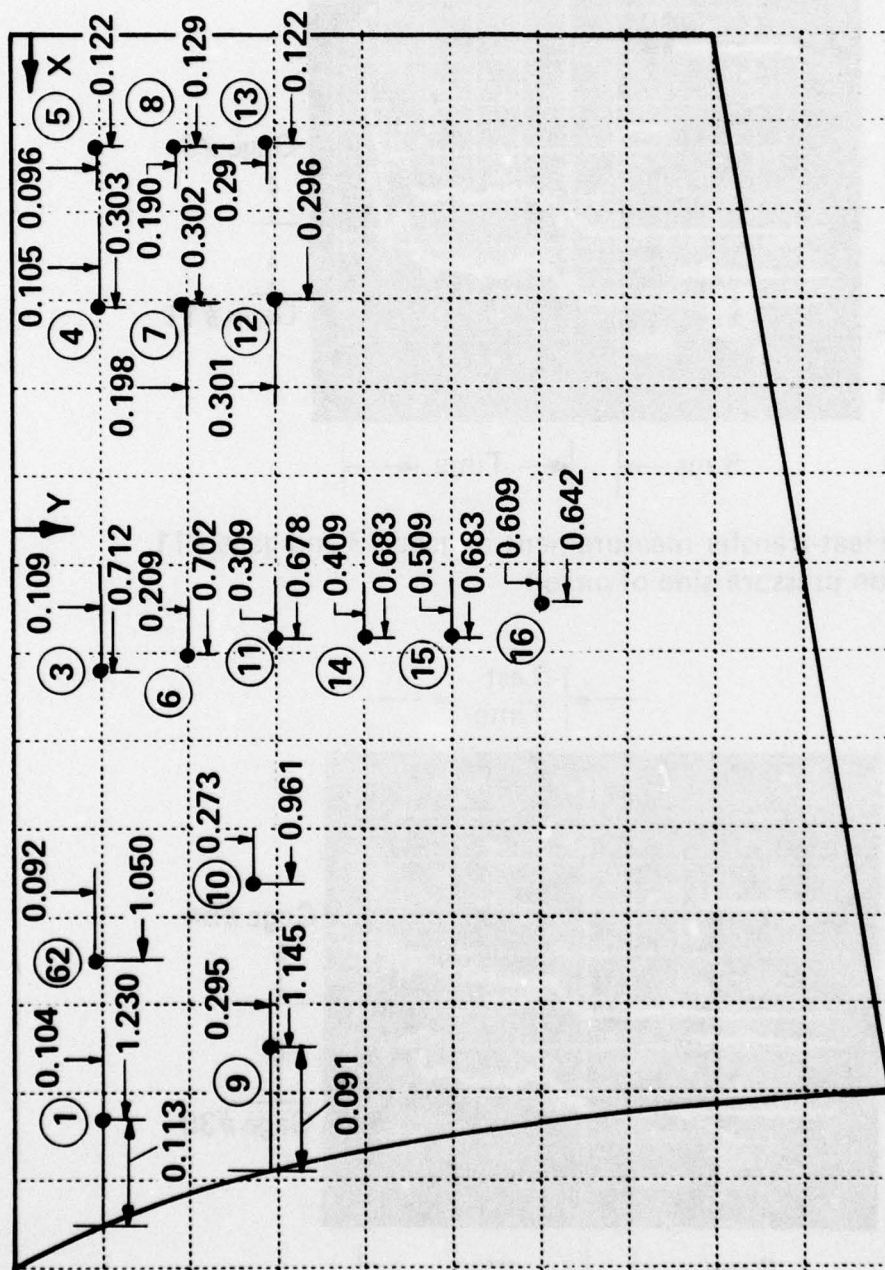


Figure 15 LOCATION OF HEAT-TRANSFER GAGES ON TIP ENDWALL



NOTE: (1) ALL DIMENSIONS ARE IN INCHES, TO  
CONVERT FROM INCHES TO METERS  
MULTIPLY BY 0.0254

Figure 16 LOCATION OF HEAT-TRANSFER GAGES ON AIRFOIL SUCTION SURFACE



NOTE: (1) ALL DIMENSIONS ARE IN INCHES; TO  
CONVERT FROM INCHES TO METERS  
MULTIPLY BY 0.0254

Figure 17 LOCATION OF HEAT-TRANSFER GAGES ON AIRFOIL PRESSURE SIDE

NOTE: TO CONVERT TO BTU/ft<sup>2</sup> sec, MULTIPLY BY 0.0102

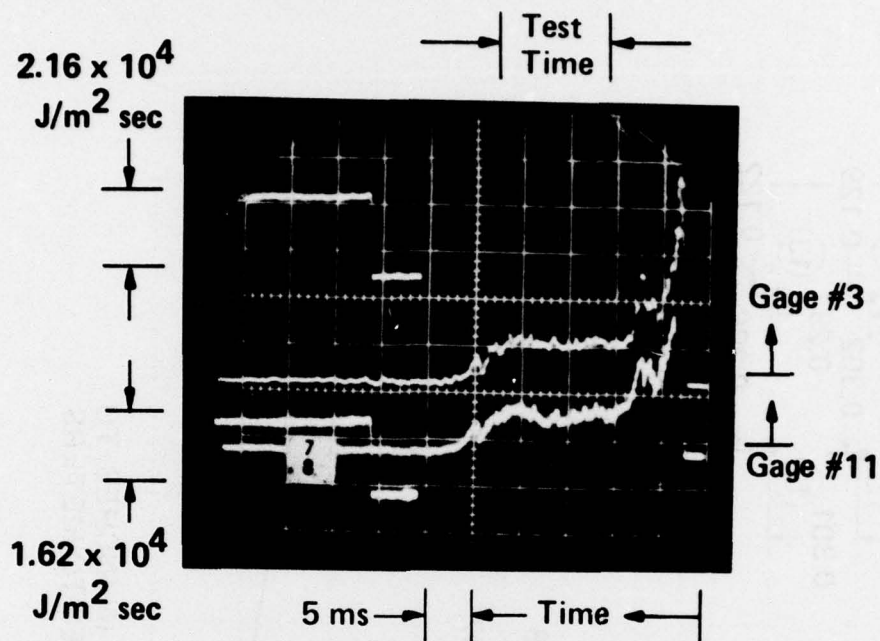


Figure 18 Heat-transfer measurement at gage #3 and gage #11 on pressure side of airfoil

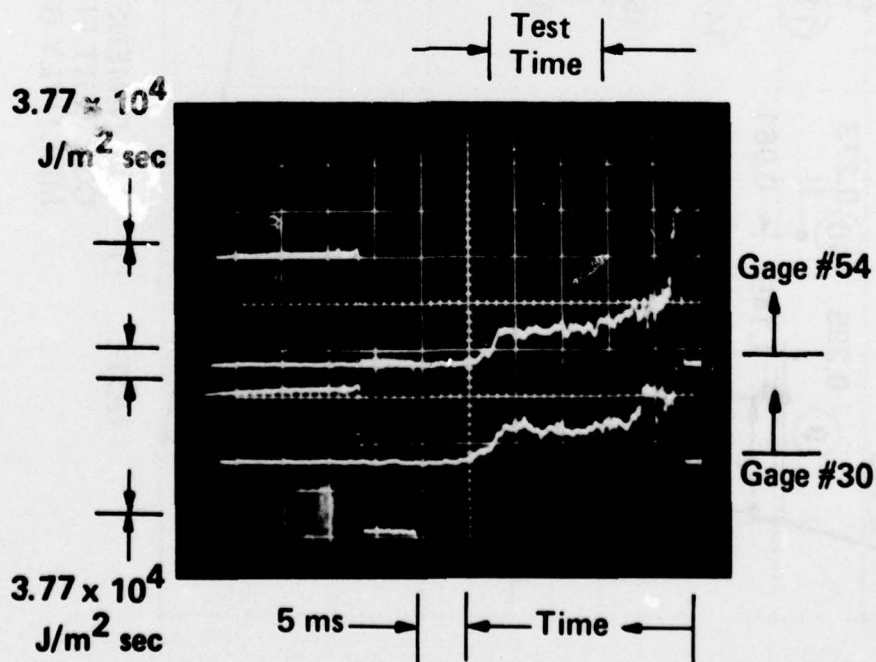


Figure 19 Heat-transfer rate on hub wall, gage #54 and on end wall, gage #30

NOTE: (1) DOTS INDICATE LOCATION OF GAGES ON FIGURES 14-23  
 (2) NUMBERS IN CIRCLE INDICATE GAGE NUMBER  
 (3) HEAT-TRANSFER RATE GIVEN BELOW GAGE IN UNITS OF  
 $\text{Joules/meters}^2 \text{ sec}$ , TO CONVERT TO  $\text{BTU/ft}^2 \text{ sec}$ ,  
 MULTIPLY BY 0.01021

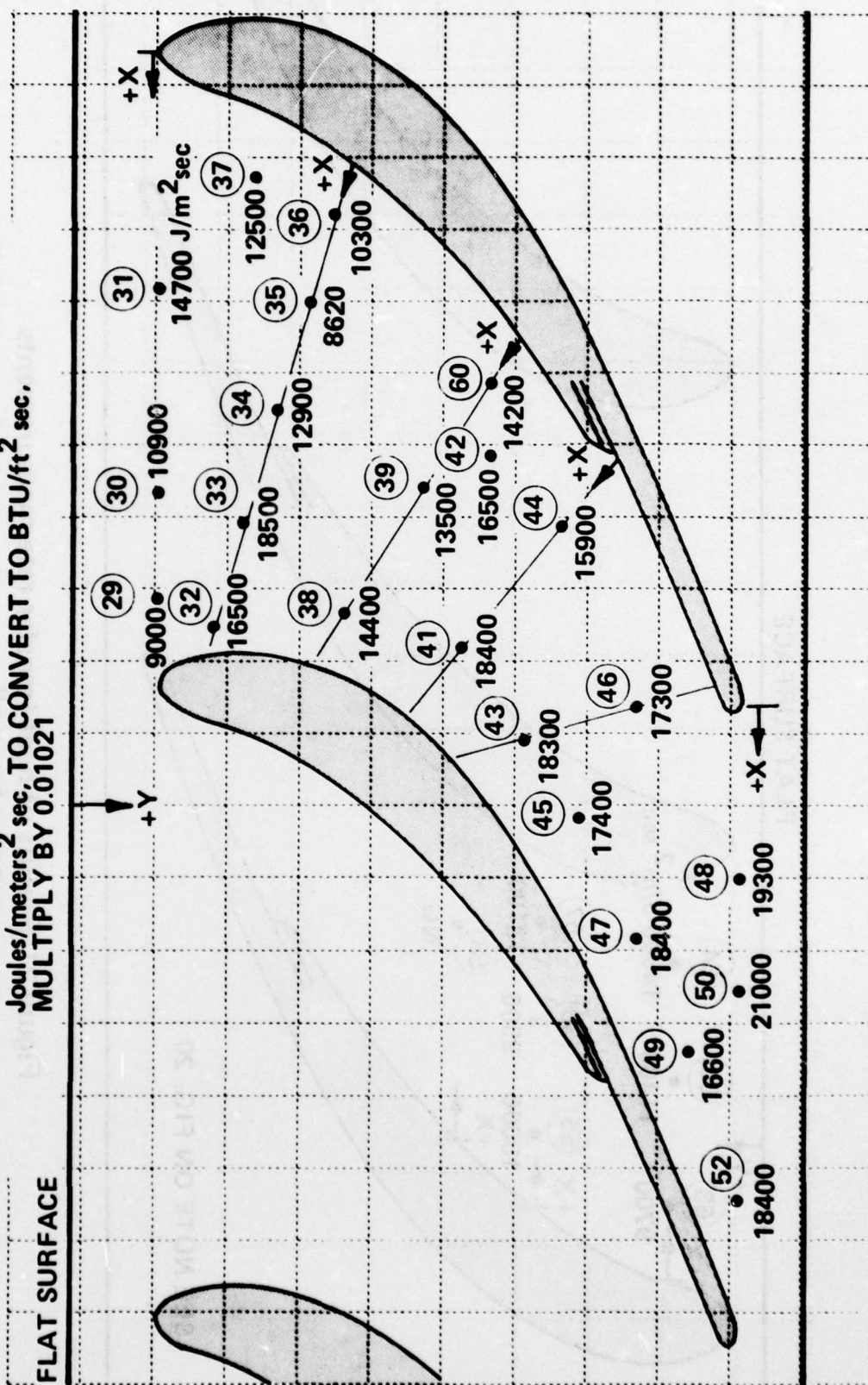


Figure 20 Results of heat-transfer rate measurement  
 on stator end wall

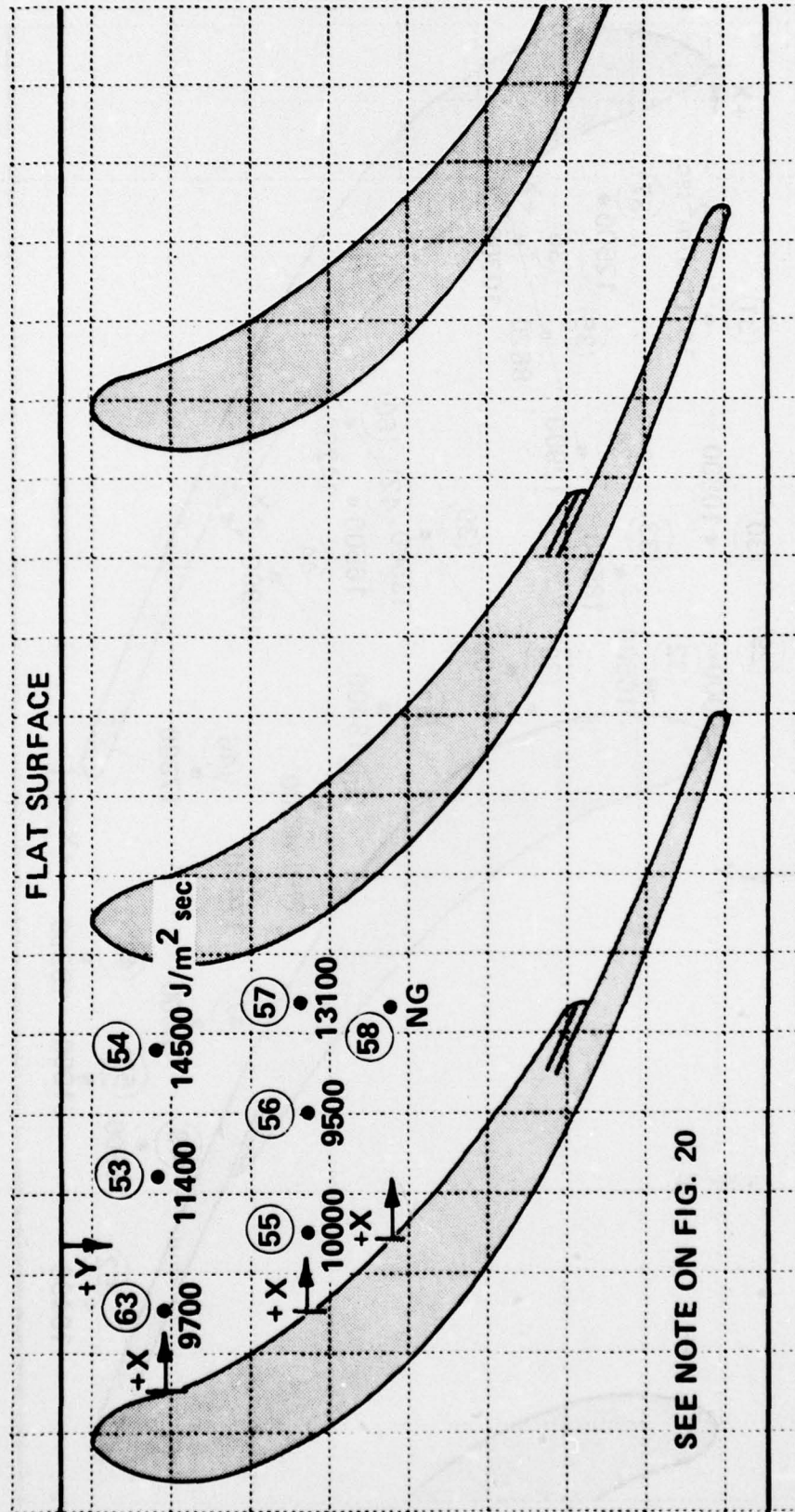


Figure 21 Results of heat-transfer rate measurements  
on stator hubwall

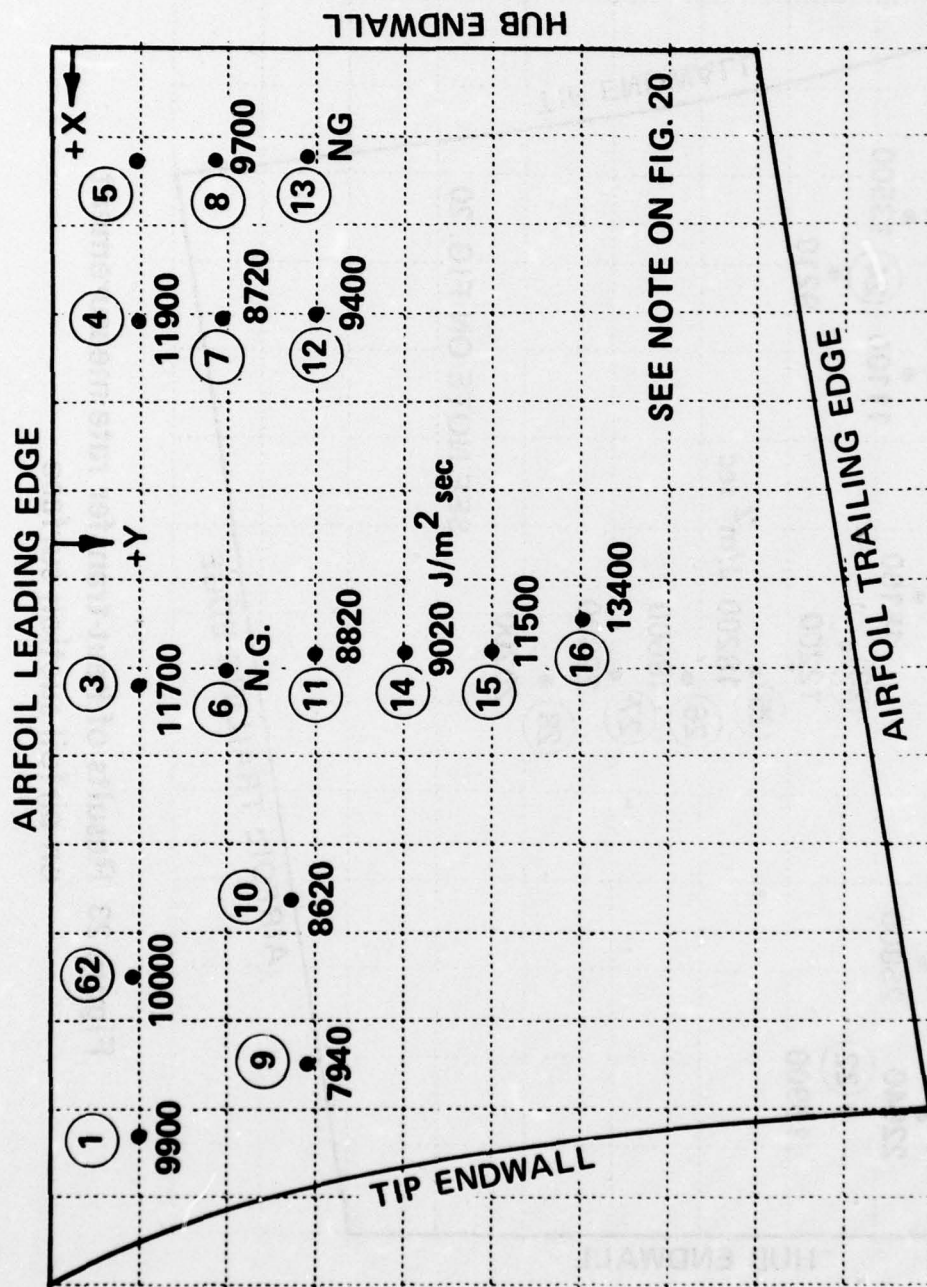


Figure 22 Results of heat-transfer rate measurements on airfoil pressure surface

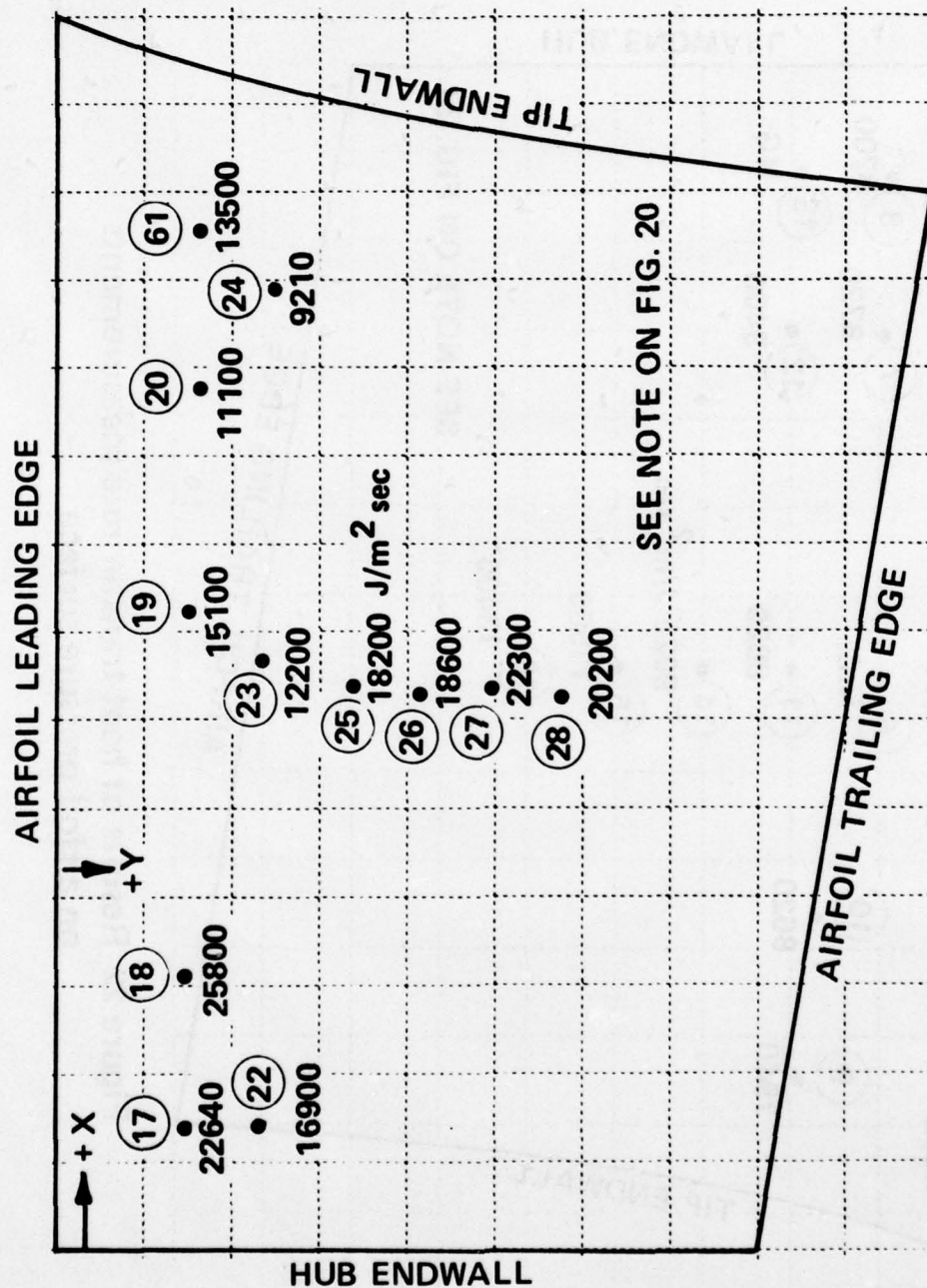


Figure 23 Results of heat-transfer rate measurement on airfoil suction surface

## REFERENCES

1. Dodge, P. R., "A Numerical Method for 2-D and 3-D Viscous Flows", AIAA 9th Fluid and Plasma Dynamics Conference, AIAA Paper No. 76-425, July 1976.
2. Katsanis, T. and McNally, W. D., "Fortran Program for Calculating Velocities in a Magnified Region on a Blade-to-Blade Stream Surface to a Turbomachine", NASA Tech. Note D-5091.
3. Wu, C. H., "A General Theory of Three-Dimensional Flow With Subsonic and Supersonic Velocity in Turbomachines Having Arbitrary Hub and Casing Shapes - Parts I and II", ASME Paper 50-A-79.
4. Smith, L. H., "Radial-Equilibrium Equations of Turbomachinery", ASME 65-AW/GTP-1.
5. Horlock, J. H. and Perkins, H. J., "Annulus Wall Boundary Layers in Turbomachines", AGARD-AG-185.
6. Blair, M. F., "An Experimental Study of Heat Transfer and Film Cooling on Large-Scale Turbine Endwalls", Transactions of the ASME, Journal of Heat Transfer, Nov. 1974, pp. 524-529.
7. Louis, J. F., "Investigation of Factors Affecting Heat Transfer to Turbine End Walls", Air Force Aero Propulsion Laboratory, TR-73-93, Oct. 1973.
8. Jones, T. V. and Schultz, D. L., "A Study of Film Cooling Related to Gas Turbines Using Transient Techniques", University of Oxford Report No. 1121/70.
9. Smith, M. R., "A Study of Film Cooling Effectiveness with Discrete Holes and Slots", University of Oxford Report No. 1100/74.
10. Hanus, G. J. and L'Ecuyer, M., "Turbine Vane Leading Edge Gas Film Cooling With Spanwise Angled Coolant Holes", AIAA Paper No. 76-43, Jan. 1976.
11. Szanca, E. M., Schum, H. J., and Behning, F. P., "Cold-Air Investigation of a Turbine with Transpiration-Cooled Stator Blades", NASA TM X-2133, Oct. 1970.
12. Gladden, H. J. et al., "Aerodynamic Investigation of Four-Vane Cascade Designed for Turbine Cooling Studies", NASA TM X-1954, Jan. 1970.

13. Calvert, H. F., et al., "Turbine Cooling Research Facility", NASA TM X-1927, March 1970.
14. Dunn, M. G. and Stoddard, F. J., "Development of a Shock-Tunnel Technique for the Measurement of Heat-Transfer Rate to Gas Turbine Components", 11th International Symposium on Shock Tubes and Waves, July 1977.
15. Dunn, M. G. and Stoddard, F. J., "Measurement of Heat-Transfer Rate to a Gas Turbine Stator", submitted for publication, Aug. 1977.
16. Perry, J. A., "Critical Flow Through Sharp-Edged Orifices", Transactions of the ASME, Oct. 1949, pp. 757-764.
17. Bontrager, P.J., "Development of Thermocouple-Type Total Temperature Probes in the Hypersonic Flow Regime", AEDC-TR-69-25, Jan. 1969.
18. Vidal, R. J., "Model Instrumentation Techniques for Heat Transfer and Force Measurements in a Hypersonic Shock Tunnel", Cornell Aeronautical Laboratory Rept. No. AD-917-A-1, Feb. 1956.
19. Wittliff, C. E., Wilson, M. R., and Hertzberg, A., "The Tailored-Interface Hypersonic Shock Tunnel", Journal of the Aerospace Sciences, Vol. 26, No. 4, April 1959, pp. 219-228.
20. Lewis, C. H. and Burgess, E. G., "Charts of Normal Shock Wave Properties in Imperfect Air (Supplement:  $M_s = 1$  to 10)", AEDC-TR-65-196, Sept. 1965.
21. Dunn, M. G., "Experimental Study of Reflected-Shock Tunnel Flows in the Equilibrium Interface Region", Cornell Aeronautical Laboratory Report AM-1702-A-1, Jan. 1968.
22. Balje, O. E., "Axial Cascade Technology and Application to Flow Path Designs, Part 1 - Axial Cascade Technology", ASME Journal of Engineering Power, Oct. 1968, pp. 309-328.
23. Skinner, G. T., "Analog Network to Convert Surface Temperature to Heat Flux", Cornell Aeronautical Laboratory Rept. No. CAL-100, Feb. 1960.
24. Dodge, P. R., "3-D Heat Transfer Analysis Program", Final Report, Air Force Aero Propulsion Laboratory Rept. No. TR-77-Sept. 1977.